Article

Cell Reports

Ontogenic shifts in cellular fate are linked to proteotype changes in lineage-biased hematopoietic progenitor cells

Graphical Abstract

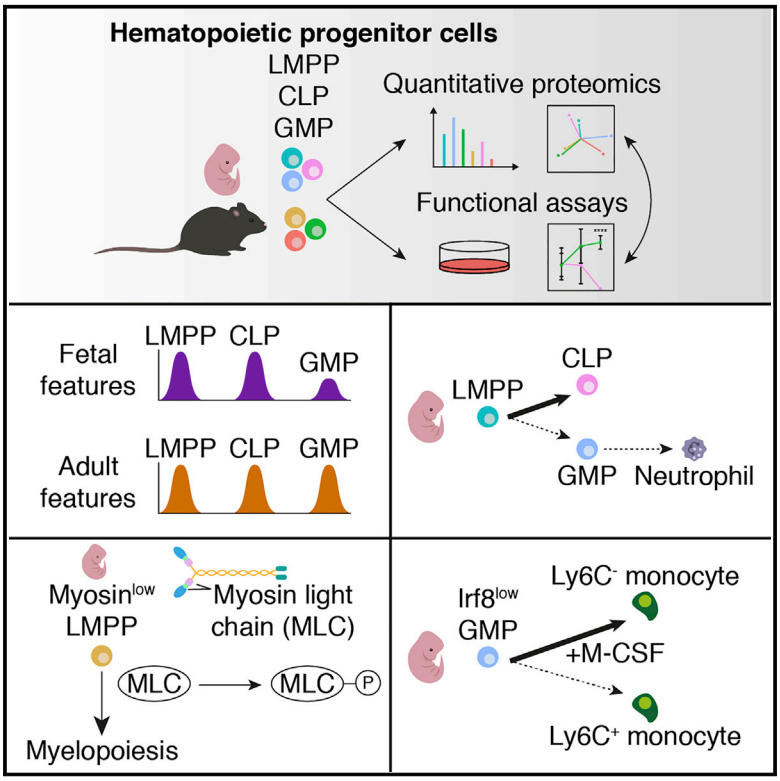

Authors

Maria Jassinskaja, Kristýna Pimková, Nejc Arh, ..., Carlos-Filipe Pereira, Ewa Sitnicka, Jenny Hansson

Correspondence

jenny.hansson@med.lu.se

In brief

Jassinskaja et al. describe ontogeny-specific proteomic signatures and functionality of lineage-biased hematopoietic progenitor cells (HPCs). They uncover that fetal-specific features differ between lymphoid-competent and myeloid-restricted progenitors and reveal an ontogenic shift in monocyte differentiation capacity, partially driven by differential Irf8 expression between fetal and adult granulocyte-monocyte progenitors (GMPs).

Highlights

- >4,000 proteins quantified in fetal and adult hematopoietic progenitor cells (HPCs)
- Protein expression in HPCs separates cells based on ontogenic stage and lineage potential
- Generic fetal features are suppressed in myeloid-restricted progenitors
- Low Irf8 expression partially drives an impairment in monopoiesis in fetal HPCs

Jassinskaja et al., 2021, Cell Reports *34*, 108894
March 23, 2021
https://doi.org/10.1016/j.celrep.2021.108894

CellPress

Cell Reports

CellPress
OPEN ACCESS

Article

Ontogenic shifts in cellular fate are linked to proteotype changes in lineage-biased hematopoietic progenitor cells

Maria Jassinskaja,[1] Kristýna Pimková,[1] Nejc Arh,[2,3] Emil Johansson,[1,4] Mina Davoudi,[1] Carlos-Filipe Pereira,[2,3] Ewa Sitnicka,[1] and Jenny Hansson[1,5,*]

[1]Lund Stem Cell Center, Division of Molecular Hematology, Lund University, 221 84 Lund, Sweden
[2]Lund Stem Cell Center, Division of Molecular Medicine and Gene Therapy, Lund University, 221 84 Lund, Sweden
[3]Wallenberg Centre for Molecular Medicine, Lund University, 221 84 Lund, Sweden
[4]Department of Laboratory Medicine, Lund University, 221 84 Lund, Sweden
[5]Lead contact
*Correspondence: jenny.hansson@med.lu.se
https://doi.org/10.1016/j.celrep.2021.108894

SUMMARY

The process of hematopoiesis is subject to substantial ontogenic remodeling that is accompanied by alterations in cellular fate during both development and disease. We combine state-of-the-art mass spectrometry with extensive functional assays to gain insight into ontogeny-specific proteomic mechanisms regulating hematopoiesis. Through deep coverage of the cellular proteome of fetal and adult lympho-myeloid multipotent progenitors (LMPPs), common lymphoid progenitors (CLPs), and granulocyte-monocyte progenitors (GMPs), we establish that features traditionally attributed to adult hematopoiesis are conserved across lymphoid and myeloid lineages, whereas generic fetal features are suppressed in GMPs. We reveal molecular and functional evidence for a diminished granulocyte differentiation capacity in fetal LMPPs and GMPs relative to their adult counterparts. Our data indicate an ontogeny-specific requirement of myosin activity for myelopoiesis in LMPPs. Finally, we uncover an ontogenic shift in the monocytic differentiation capacity of GMPs, partially driven by a differential expression of Irf8 during fetal and adult life.

INTRODUCTION

The lifelong support of the entire blood system relies on a complex differentiation program of hematopoietic stem cells (HSCs) and their progeny. The process of hematopoiesis occurs in waves with distinguishable functional characteristics from embryonic development through adulthood (Babovic and Eaves, 2014; Jassinskaja et al., 2017; Mikkola and Orkin, 2006). In mice, the largest burst of fetal hematopoiesis occurs in the fetal liver (FL) at embryonic day 14.5 (E14.5) (Ema and Nakauchi, 2000; Kieusseian et al., 2012; Morrison et al., 1995). Before birth, hematopoietic stem and progenitor cells (HSPCs) from the FL begin to populate the bone marrow (BM), where hematopoiesis is maintained after birth and throughout the lifetime of the animal (Babovic and Eaves, 2014).

Fetal and adult HSPCs exhibit substantial differences in several key functional aspects, such as cell cycle kinetics (Ema and Nakauchi, 2000; Jassinskaja et al., 2017; Rebel et al., 1996), response to inflammatory stress (Jassinskaja et al., 2017; Kim et al., 2016), and output of various blood and immune cell subsets (Bendelac et al., 2001; Hardy and Hayakawa, 1991; Rowe et al., 2016). The molecular programs that govern the functional differences between fetal and adult hematopoiesis have predominantly been investigated at the transcript level in HSCs (Beerman et al., 2014; Manesia et al., 2017; McKinney-Freeman et al., 2012). However, since post-transcriptional regulation has a vital role in HSPC function, both under normal and non-homeostatic conditions (Haas et al., 2015; Jassinskaja et al., 2017; Klimmeck et al., 2012; Raffel et al., 2020; Sun et al., 2018; Zaro et al., 2020), comprehensive protein-level characterization is essential for delineating the molecular mechanisms regulating the functional variation of hematopoiesis during normal development and disease. In our previous work, we established that the proteome of Lin^- $Sca\text{-}1^+$ $cKit^+$ (LSK) HSPCs undergoes extensive ontogenic remodeling that is reflective of the divergent nature of fetal and adult hematopoiesis (Jassinskaja et al., 2017). Studies on such heterogeneous populations of cells provide an excellent overview of fetal- and adult-specific features that are shared among many early hematopoietic cells. Nevertheless, the molecular programs that orchestrate important functions related to differentiation capacity and lineage-bias during ontogeny and disease remain unresolved.

Although a discrete hierarchical organization of hematopoiesis is subject to debate (Velten et al., 2017), mature lymphoid and myeloid cell development is widely considered to occur through the differentiation of HSCs via several downstream hematopoietic progenitor cells (HPCs), including a progenitor with lympho-myeloid potential (lympho-myeloid multipotent progenitor

[LMPP]), which gives rise to progenitors largely restricted toward the lymphoid (common lymphoid progenitor [CLP]) or myeloid (granulocyte-monocyte progenitor [GMP]) lineage (Nimmo et al., 2015). Importantly, lineage-biased HPCs represent a critical target for proteomic investigation because such cells can act as highly potent leukemia-initiating cells (Ugale et al., 2014). In addition, twin studies and retrospective analyses of neonatal blood tests have unequivocally shown that infant leukemia is frequently already initiated in utero (Greaves et al., 2003). Considering that, it is particularly intriguing that acute leukemia predominately manifests as a lymphoid disease in infants, whereas myeloid leukemias are more common in adults (Meyer et al., 2018). Furthermore, recent findings indicate that this difference in incidence of leukemias of different lineages in children and adults, at least in part, originates from a differential susceptibility to leukemic transformation in lineage-biased HPCs at distinct stages of ontogeny (Böiers et al., 2018).

Here, we report a characterization of ontogenic changes that occur in the cellular proteome of immunophenotypic LMPPs, CLPs, and GMPs. We have quantified more than 4,000 proteins and uncovered striking differences between the fetal and the adult cells in the expression of hundreds of proteins. Through extensive functional assays, we link the proteomic signatures to cellular phenotypes and illuminate ontogenic differences in the molecular makeup and functionality of lineage-biased HPCs.

RESULTS

Immunophenotypic LMPPs, CLPs, and GMPs exhibit ontogeny-specific lineage output and differentiation kinetics

The immunophenotype and lineage-potential of murine adult LMPPs, CLPs and GMPs have been extensively studied (Adolfsson et al., 2005; Karsunky et al., 2008; Månsson et al., 2007; Pietras et al., 2015; Pronk et al., 2007; Richie Ehrlich et al., 2011), whereas less is known about the cells' counterparts during fetal life. Using the immunophenotypic definitions previously described for the adult hematopoietic hierarchy (Adolfsson et al., 2005; Karsunky et al., 2008; Månsson et al., 2007; Pietras et al., 2015; Pronk et al., 2007), we first determined the occurrence of LMPPs (LSK $Flt3^{high}$ $CD150^{-}$), CLPs (Lin^{-} $Sca\text{-}1^{low}$ $cKit^{low}$ [$LS^{low}K^{low}$] IL-7Ra^{+} $Flt3^{high}$) and GMPs (Lin^{-} $Sca\text{-}1^{-}$ $cKit^{+}$ [$LS^{-}K$] $CD41^{low}$ $CD150^{-}$ $CD16/32^{+}$) in E14.5 FL and adult BM (ABM; 6–10 weeks old; Figures 1A–1C and S1A). The frequency of GMPs was greater than 0.1% in both tissues, whereas LMPPs and CLPs comprised less than 0.1% of the FL and ABM (Figure 1B). For the rarest cell subset (CLPs), those percentages translate to approximately 1,400 and 6,000 cells per embryo and adult mouse, respectively (Figure 1C).

We next evaluated *in vitro* lineage potential of the six cell populations under conditions promoting either B and myeloid or T cell fate (Figures 1D–1H and S1A). Analysis of the progeny of LMPPs revealed myeloid as well as B and T cell potential in both the fetal and the adult cells (Figure 1E), as previously described (Månsson et al., 2007). Compared with fetal LMPPs, adult LMPPs displayed a greatly increased capacity to generate granulocytes, producing very high frequencies of neutrophils after 12 days of culture (Figure 1E). From CLPs, B cell output was observed already after 5 days from both fetal and adult cells, and T cells were potently produced in parallel cultures (Figure 1F). We additionally detected monocytes in adult CLP wells, in line with previous reports of the OP9 co-culture system strongly promoting myelopoiesis even in *in vivo* lymphoid-restricted progenitors (Richie Ehrlich et al., 2011). Critically, fetal CLPs showed exceedingly low monocyte production (Figure 1F), suggesting stronger lineage restriction. GMPs from fetuses and adults exclusively generated myeloid cells (Figure 1G). Surprisingly, we observed almost no monocytes in wells seeded with GMPs, despite our system supporting monocytic differentiation from other progenitor subtypes (Figures 1E and 1F). Suspension culture of GMPs in the presence of macrophage-colony stimulating factor (M-CSF) demonstrated that both fetal and adult GMPs have the potential to generate monocytes (Figure 1H). Collectively, our data reveal ontogeny-specific variation in the differentiation kinetics and cell-intrinsic lineage bias of fetal and adult HPCs in the form of stronger myeloid potential in adult LMPPs and CLPs relative to their fetal counterparts, as well as a differential output of neutrophils from fetal and adult GMPs.

The proteomic landscapes of LMPPs, CLPs, and GMPs undergo extensive ontogenic remodeling

Having confirmed differential lineage potential of fetal and adult HPCs, we moved on to determine the proteomic profiles of these cells. To circumvent issues related to sample loss, we used the recently introduced in-StageTip (iST)-based methods for sample preparation (Kulak et al., 2014) and high-pH reverse-phase (HpH-RP) pre-fractionation (Dimayacyac-Esleta et al., 2015), in combination with isobaric labeling and a synchronous precursor scanning (SPS)-MS3 method enabling highly accurate quantification of six samples in one analysis (Rauniyar and Yates, 2014) (Figures 2A, S1B, and S1C). We subjected 100,000 fluorescence-activated cell sorting (FACS)-purified LMPPs, CLPs, and GMPs (Figures 1A and S1A) from E14.5 FL and ABM in three biological replicates to our proteomic workflow (Figures 2A, S1B, and S1C). We identified 4,189 proteins, of which 4,021 proteins (96%) were quantified in all six cell populations (Figures S1D and S1E; Table S1). The cellular proteomes showed a high dynamic range and a broad expression profile over the six cell subsets (Figure 2B).

To generate an overview of the relationship between the proteomic signatures, we performed a principal component analysis (PCA; Figure 2C). Although the PCA segregated CLPs as well as LMPPs on ontogenic stage, these two lymphoid-competent progenitors positioned close to each other for FL and ABM, respectively, illuminating particularly strong fetal- and adult-specific features in LMPPs and CLPs. Conversely, the rather close positioning of fetal and adult GMPs points toward stronger ontogenic conservation in this cell type. Upon analysis of which proteins contributed most to the separation in the PCA, we found, as expected, that generic fetal signatures included known fetal-enriched proteins, such as transcription factor (TF) Arid3a (Zhou et al., 2015), and insulin-like growth factor-binding proteins (Igf2bp1, Igf2bp2, and Igf2bp3) (Jassinskaja et al., 2017; Zhang and Lodish, 2004). Adult characteristics covered proteins related to antigen presentation (e.g., H2-K1, H2-D1, and B2m), which we have previously shown to be higher expressed in adult

CellPress
OPEN ACCESS

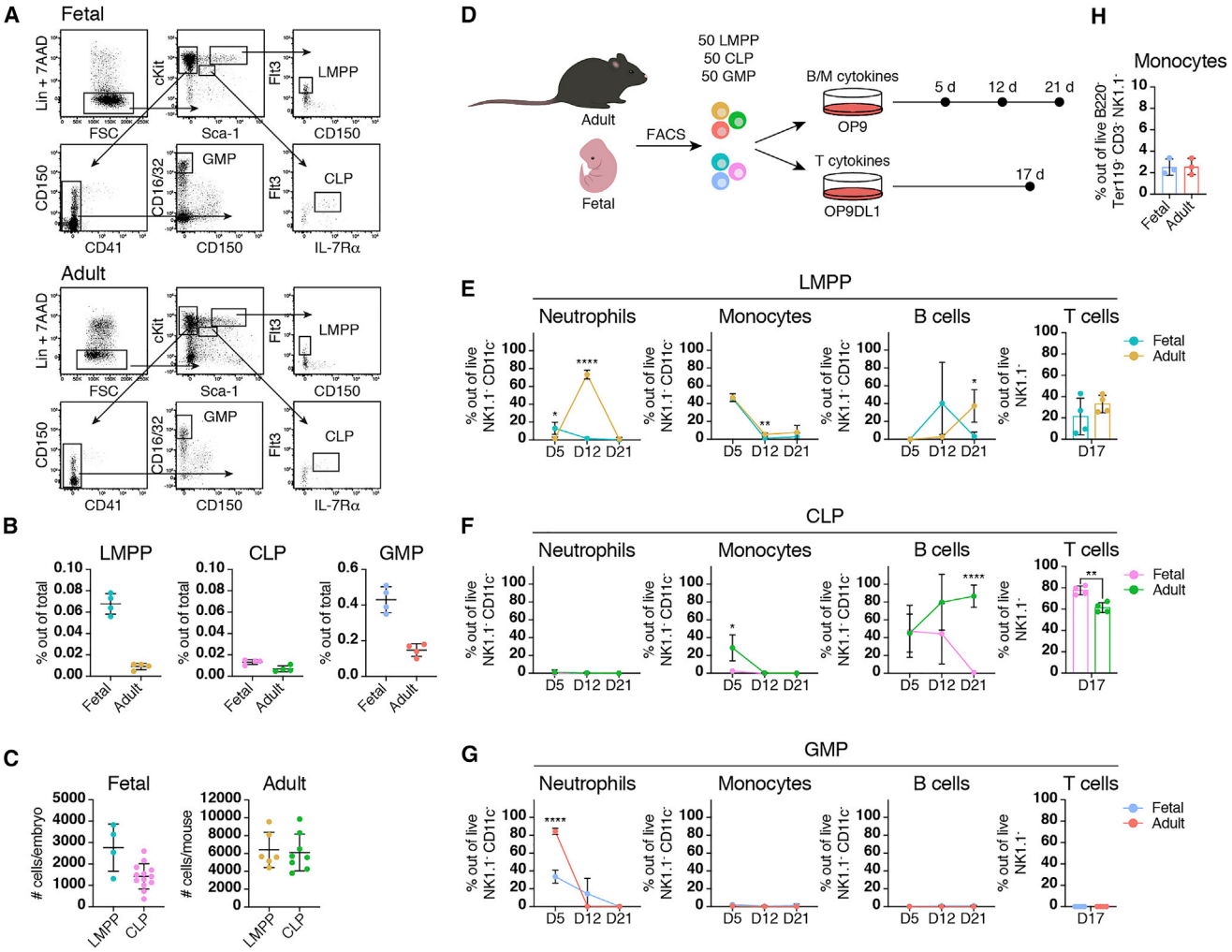

Figure 1. Fetal and adult HPCs show distinct lineage potential and differentiation kinetics

(A) Representative FACS plots showing the gating strategy for LMPPs (LSK Flt3^{high} CD150^{-}), CLPs (LS^{low}K^{low} Flt3^{+} IL7R^{+}), and GMPs (LS^{-}K CD41^{low} CD150^{-} CD16/32^{+}) in E14.5 FL and ABM.

(B) Frequency of LMPPs, CLPs, and GMPs in E14.5 FL and ABM. n = 4.

(C) Number of LMPPs and CLPs present in one embryo and one adult mouse (hind limbs, forelimbs, spine, and sternum) extrapolated from FACS sorting. n = 4, 13, 6, and 8 for fetal LMPPs, fetal CLPs, adult LMPPs, and adult CLPs, respectively.

(D) *In vitro* differentiation workflow for evaluation of fetal and adult LMPP, CLP, and GMP lineage potential.

(E–G) Frequency of neutrophils (NK1.1^{-} CD11c^{-} CD11b^{+} Ly6G^{+}), monocytes (NK1.1^{-} CD11c^{-} CD11b^{+} CD115^{+}), B cells (NK1.1^{-} CD11c^{-} CD11b^{-} CD19^{+} B220^{+}), and T cells (NK1.1^{-} Thy1^{+} CD25^{+} and/or NK1.1^{-} CD4^{+} CD8^{+}) at different time points in wells seeded with fetal and adult LMPPs (E), CLPs (F), and GMPs (G). n = 4.

(H) Frequency of monocytes after 7-day suspension culture of fetal and adult GMPs. n = 3.

Error bars represent means ± SD. *p < 0.05, **p < 0.01, ***p < 0.001, ****p < 0.0001. See also Figure S1.

compared with fetal HSPCs (Jassinskaja et al., 2017) (Figure S1F). Glycolysis-associated protein pyruvate kinase (Pklr) contributed equally to both the fetal LMPP and CLP signatures. The fetal LMPP signature was additionally strongly influenced by Lin28b-target Hmga2 (Rowe et al., 2016), whereas lymphopoiesis-associated proteins, such as Grap2 (Ma et al., 2001), Bcl11a (Yu et al., 2012), and Lsp1 (Carballo et al., 1996), contributed to the signature of fetal CLPs. Intriguingly, another protein causative to the separation of fetal CLPs from the other cell populations was alpha-hemoglobin stabilizing protein (Ahsp). This molecular chaperone has a well-documented role in erythropoiesis (Feng et al., 2004), but its function within the context of lymphopoiesis has not been described. Among proteins contributing to the fetal GMP signature, we identified the pro-inflammatory protein S100a9 and, interestingly, megakaryocyte protein Stfa1 (Mezzapesa et al., 2019). The adult LMPP signature included Stat3-activator Ociad2 (Sinha et al., 2018), whereas adult lymphopoiesis-specific enzyme Dntt (Jassinskaja et al., 2017) contributed strongly to the signature of adult CLPs. Surprisingly, the proteomic signatures of adult LMPPs and CLPs

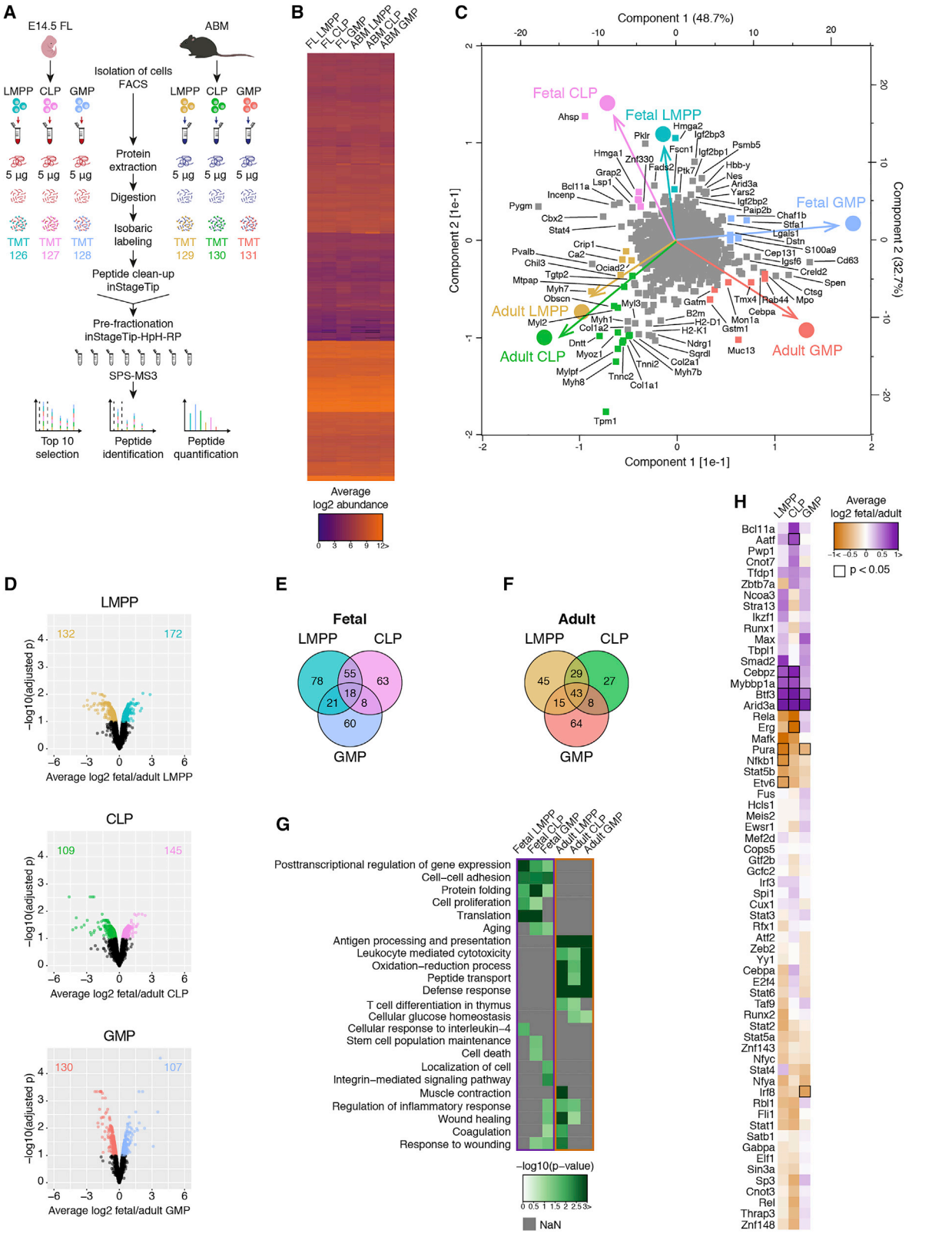

(legend on next page)

were additionally strongly influenced by several members of the myosin, tropomyosin, and troponin family of proteins (e.g., Mylpf, Myoz1, Tpm1, Myh7, Myh7b, and Myl2), a, to our knowledge, previously unknown hallmark of adult versus fetal lymphoid-competent progenitors. Comparison with RNA data on neonatal and adult CLPs with an alternative immunophenotypic definition suggested that the ontogeny-specific expression of myosins is regulated post-transcriptionally (data not shown). Myelopoiesis-associated proteins (e.g., Cebpa, Mpo, and Rab44) (Kadowaki et al., 2020; Scott et al., 1992), as well as redox proteins Tmx4 and Gstm1 could be found to represent features of adult GMPs.

Differential protein expression between fetal and adult HPCs is predictive of ontogenic changes in functionality

In contrast to upstream HPCs, which display considerably greater proteome complexity in adult, relative to the fetus (Jassinskaja et al., 2017), HPCs showed balanced distribution of differentially expressed proteins (Figure S1G), indicating a similar level of proteome complexity in these cells across ontogeny. Statistical analysis of proteins quantified in at least two replicates identified 304, 254, and 237 proteins as differentially expressed between fetal and adult LMPPs, CLPs, and GMPs, respectively (adjusted pvalue < 0.05; Figure 2D). As already indicated by PCA (Figure 2C), the number of differentially expressed proteins establish GMPs as the least ontogenically distinct cell type. Proteins significantly higher expressed in fetal LMPPs and CLPs compared with their adult counterparts showed a high overlap (55 proteins), whereas only 18 proteins were shared among all three fetal cell types (Figure 2E). The corresponding numbers in the adult were 29 and 43 proteins, respectively (Figure 2F), demonstrating that adult-specific features are conserved across different hematopoietic lineages, whereas fetal-specific features diverge between lymphoid-competent and myeloid-restricted progenitors.

Gene Ontology (GO) enrichment analysis of differentially expressed proteins showed that common features of proteins higher expressed in fetal HPCs are related to translation (mainly ribosomal proteins) and cell-cell adhesion (e.g., Lgals9, Lgals1, Fscn1, S100a8, S100a9, and Plek) (Figures 2G and S1H). Proteins higher expressed in adult HPCs were instead enriched for immune-response-related processes and oxidation-reduction processes (mainly glycolytic proteins and proteins involved in glutathionylation), as previously reported by us and others for adult HSPCs (Jassinskaja et al., 2017; McKinney-Freeman et al., 2012). In line with the adult LMPP signature in our PCA (Figure 2C), "muscle contraction" was enriched in proteins significantly higher expressed in adult LMPPs and included Myh1, Myl1, and Myh4, among others. Interestingly, fetal GMPs were the only cell type in the fetus in which differentially expressed proteins showed enrichment for multiple processes related to inflammation (e.g., "regulation of inflammatory response," "coagulation," and "wound healing"; Figures 2G and S1H), including proteins such as Apoe, Plek, Vcl, and Ptk7. This suggests that fetal GMPs are more strongly intrinsically poised to quickly react to inflammatory insult compared with their adult counterpart.

To further delineate functionally relevant protein expression differences, we next performed an analysis of TFs. We found differential expression of known regulators of hematopoiesis (Arid3a, Erg, Nfkb1, Etv6, and Irf8), as well as several TFs with yet poorly described or undefined functions in early blood cell development (Aatf, Cebpz, Mybbp1a, Btf3, and Pura; Figures 2H and S2A). In addition to confirming the requirement of Erg in adult B lymphopoiesis (Loughran et al., 2008; Ng et al., 2011, 2020), the expression profile of this TF excludes it as a major driver of fetal lymphopoiesis (Figure S2A). Intriguingly, Btf3—a TF with no defined role in hematopoiesis—followed the same expression pattern as the known fetal-enriched TF Arid3a (Zhou et al., 2015) (Figure 2H), highlighting its potential role as a regulator of fetal-specific features of hematopoiesis. Btf3 has been suggested to act as an inhibitor of the Nfκb signaling pathway (Kusumawidjaja et al., 2007), of which we found a major part to be downregulated in fetal compared with adult HPCs (Figure S2B). Importantly, Mybbp1a, which we identified as significantly higher expressed in fetal LMPPs and CLPs compared with their adult counterparts (Figure 2H), has also been implicated as a Nfκb repressor (Owen et al., 2007), suggesting that several mechanisms function to dampen inflammatory responses driven by Nfκb in fetal HPCs.

Differential expression of myosin-family proteins distinguishes fetal and adult LMPPs

One of the main proteomic features distinguishing fetal and adult LMPPs was a significantly greater expression of many members of the myosin, tropomyosin, and troponin family of proteins in the

Figure 2. Ontogenic remodeling of the proteome of LMPPs, CLPs, and GMPs

(A) Workflow for proteomic analysis of fetal and adult LMPPs, CLPs, and GMPs. iST-based methods were used for sample preparation (Kulak et al., 2014) and HpH-RP pre-fractionation (Dimayacyac-Esleta et al., 2015). Samples were labeled with isobaric tags and analyzed by mass spectrometry using an SPS-MS3 method (Rauniyar and Yates, 2014).

(B) Heatmap depicting the average abundance of 4,032 proteins quantified in at least one cell population.

(C) PCA of relative protein expression. Colored proteins likely contribute the most to the separation.

(D) Statistical analysis of proteins differentially expressed between fetal and adult LMPPs, CLPs, and GMPs. Proteins with significantly greater expression (adjusted p value < 0.05) are shown in color.

(E and F) Overlap of proteins significantly higher expressed in fetal (E) and adult (F) cells.

(G) Heatmap showing selected results from GO analysis of biological processes enriched in differentially expressed proteins. Only processes with a p value < 0.05 are shown. Processes that were not detected are depicted in gray. See Figure S1H for a full depiction of enriched biological processes.

(H) Heatmap depicting the relative expression of proteins classified as transcription factors by PANTHER (Mi et al., 2019) and validated by TRRUST (Han et al., 2018). Proteins differentially expressed between fetus and adult are indicated with a black frame. All expression data represent the average of three biological and two technical replicates.

See also Figures S1 and S2 and Table S1.

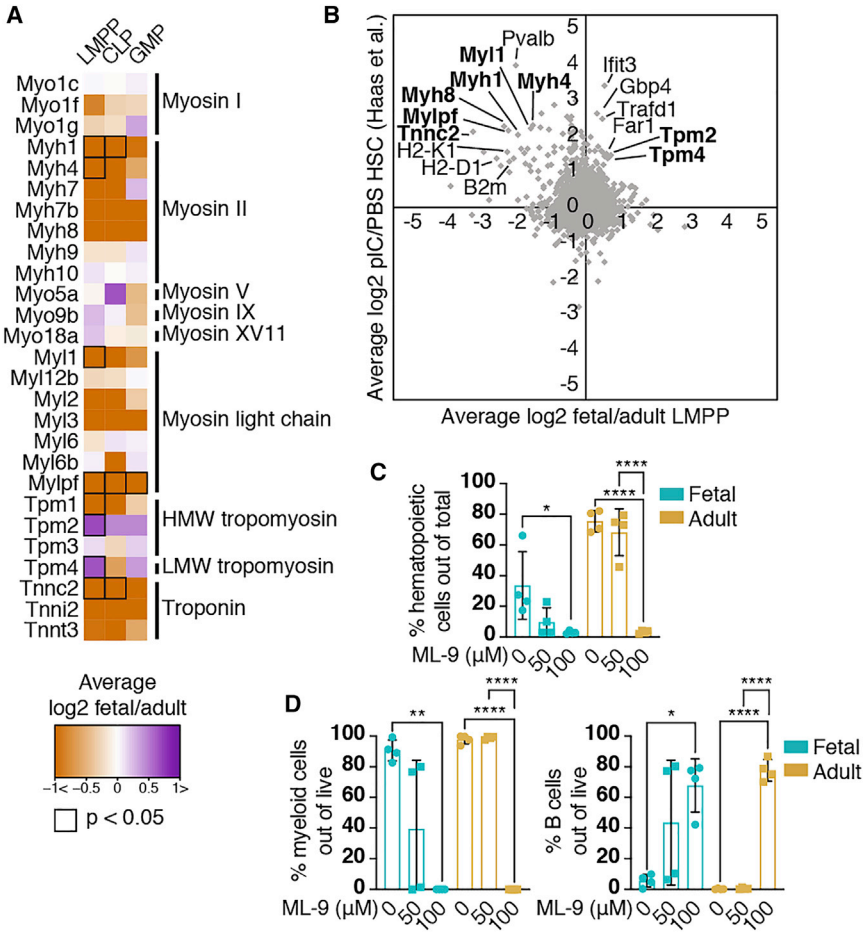

Figure 3. Fetal and adult LMPPs exhibit differential sensitivity to ROCK inhibition

(A) Average expression of proteins belonging to the myosin, myosin light chain, tropomyosin and troponin family of proteins in fetal and adult LMPPs, CLPs, and GMPs. Differentially expressed proteins are indicated with a black frame. HMW, high molecular weight; LMW, low molecular weight. n = 3.

(B) Correlation between fetal/adult LMPP protein ratios and poly(I:C)/PBS-treated HSC protein ratios (Haas et al. 2015). Proteins belonging to the myosin, tropomyosin, or troponin family of proteins are indicated in bold. n = 3.

(C and D) Frequency of hematopoietic cells (C) and myeloid and B cells (D) after treatment with ML-9. n = 4. Error bars are ±SD. *p < 0.05, **p < 0.01, ****p < 0.0001.

See also Figure S2.

adult cells (Figure 3A). An intriguing role of these proteins has been described in the context of acute myeloid leukemia (AML), in which knockdown of myosin light chain (MLC) prolonged survival of leukemic mice (Mali et al., 2011). In addition, myosin activity has been implicated in inflammation (Georgouli et al., 2019), and the expression of this protein family is upregulated during emergency hematopoiesis toward the myeloid and megakaryocytic lineage (Haas et al., 2015) (Figure 3B). Considering the strong ontogenic expression difference, we hypothesized that fetal and adult LMPPs may exhibit a differential dependency on myosin activity for expansion and/or myeloid differentiation. We first targeted the actin/myosin motor by interfering with MLC phosphorylation via inhibition of Rho kinase (ROCK) (Jacobs et al., 2006; Mali et al., 2011). From two independent experiments, inhibition of myosin activity reduced expansion of adult LMPPs in one of the experiments (Figure S2C) and modestly enhanced granulopoiesis in adult, but not fetal, LMPPs ($p = 0.15$ and $p = 0.03$ for adult and $p = 0.27$ and $p = 0.52$ for fetal LMPPs, respectively; Figure S2D). Strikingly, targeting of MLC kinase with the inhibitor ML-9 (Saitoh et al., 1987), at a 100-μM dose, dramatically reduced the expansion of fetal, as well as adult, LMPPs (Figure 3C). Additionally, myelopoiesis was entirely absent in treated wells, whereas B cell differentiation was greatly enhanced (Figure 3D). Interestingly, fetal cells already indicated greater sensitivity to decreased myosin activity by adverse effects at a 50-μM ML-9 dose. Because myosins have been shown to be upregulated upon acute inflammatory stress in HSCs (Figure 3B) (Haas et al., 2015), we next investigated the myeloid output of fetal and adult LMPPs after stimulation with interferon alpha (IFNα). We did not observe any difference in granulocyte output between fetal and adult LMPPs (Figure S2E), indicating that emergency granulopoiesis is regulated independently of homeostatic myosin expression levels in LMPPs. Collectively, our results highlight a potential ontogeny-specific sensitivity to loss of myosin activity in LMPPs. Detailed mechanistic dissection of myosin function and activity in LMPPs is needed to confirm these initial results and to gain further understanding of their possible role.

Proteotype of fetal and adult HPCs accurately predicts ontogenic changes in myeloid potential, whereas MegE potential is uncoupled from protein signature

We next investigated the relationship between differentially expressed proteins and lineage bias. We mapped differentially expressed proteins to transcriptional profiles of various subsets of mouse adult hematopoietic cells (Bagger et al., 2019) (Figures 4A–4C and S3A), as well as expression of individual proteins known to be involved in lineage commitment (Figure 4D). Using this approach for proteins differentially expressed between CLPs and GMPs in the fetus and adult showed, as expected, great similarity between the profiles with a clear association of proteins higher expressed in CLPs and GMPs to lymphoid and myeloid cell subsets, respectively, validating the accuracy of the approach (Figure S3A). In addition, a high correlation was observed between fetal and adult CLP versus GMP protein

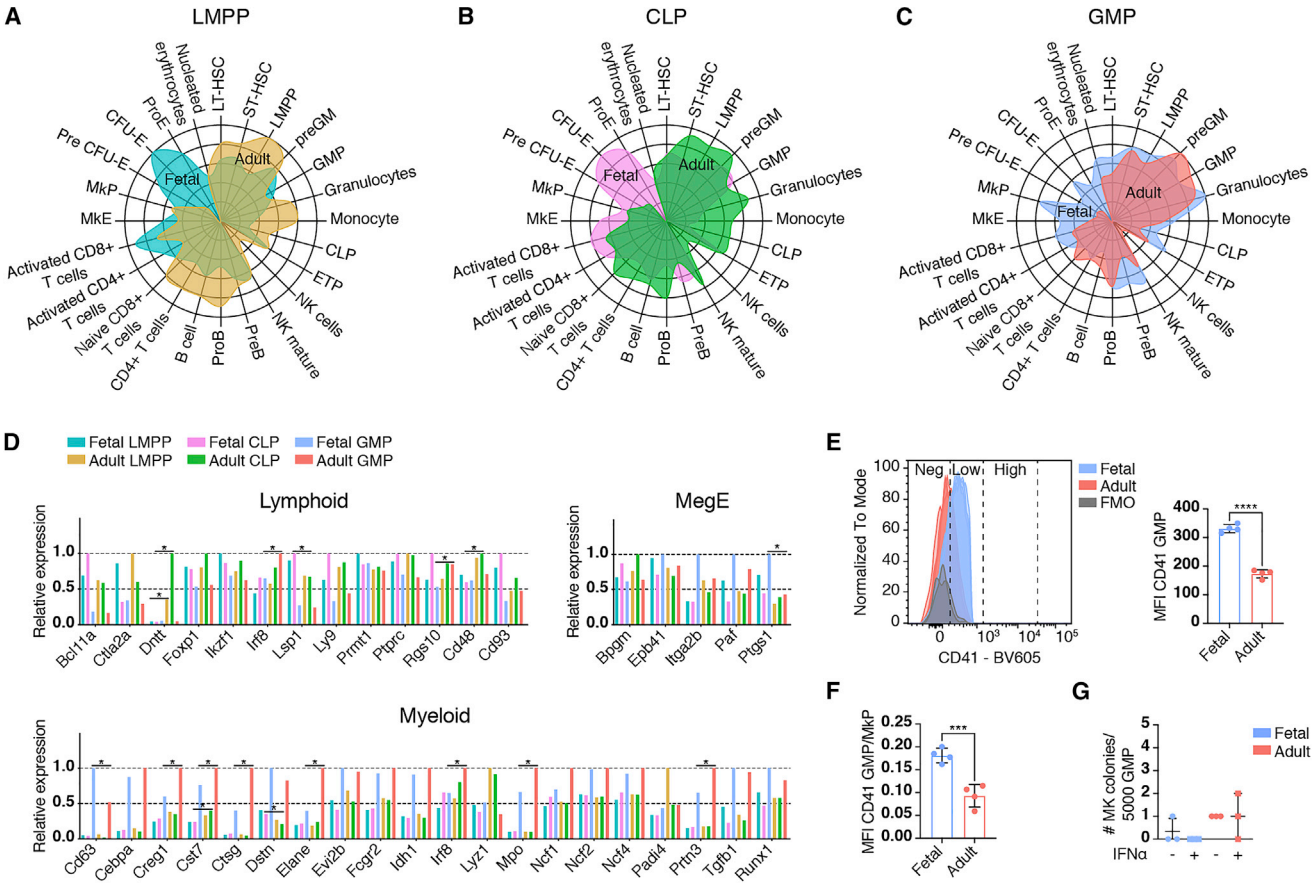

Figure 4. Proteomic profiles predict differential functionality and lineage potential of fetal and adult HPCs

(A–C) Radar plots depicting the association of differentially expressed proteins in LMPPs (A), CLPs (B), and GMPs (C) with known transcriptional profiles of murine hematopoietic cell subsets.

(D) Relative expression of proteins associated with the lymphoid, myeloid, and MegE lineage. Data represent the average of three biological replicates. *$p < 0.05$.

(E) CD41 expression on fetal and adult GMPs. FMO, fluorescence minus one. MFI, median fluorescent intensity. n = 4.

(F) CD41 expression on fetal and adult GMPs relative to MkPs. n = 4.

(G) Megakaryocte (MK) potential in fetal and adult GMPs with or without IFN-α treatment. MFI, median fluorescent intensity. n = 3.

Error bars are ±SD. ***$p < 0.001$, ****$p < 0.0001$. See also Figure S3.

expression signatures (Figure S3B), demonstrating that the main features that discriminate lymphoid from myeloid cell fate are retained during ontogeny. The retained lymphoid and myeloid signatures consisted of proteins such as Pygm, Cbx2, and Incenp and Spen, Rab44, and Cebpa, respectively (Figure S3C). Notably, despite sustained lineage commitment signatures, we found strong ontogeny-specific differences in the expression of myelopoiesis-associated proteins, where fetal GMPs showed significantly lower expression of several proteins linked to myeloid commitment, such as Irf8 (as previously noted in our analysis of TFs; Figure 2H), Mpo, and Elane (Figure 4D), compared with adult GMPs. In line with our *in vitro* differentiation data (Figures 1E and 1F), proteins higher expressed in adult LMPPs and CLPs associated more strongly with mature myeloid cell subsets compared with the corresponding fetal signatures (Figures 4A and 4B). Among individual proteins known to be involved in myelopoiesis, Cst7 was significantly higher expressed in adult CLPs compared with fetal CLPs (Figure 4D). Intriguingly, compared with the adult, fetal LMPP and CLP signatures showed a high association with the erythroid lineage (Figures 4A and 4B). We found no capacity for erythroid differentiation in either of these cell types (Figure S3D), suggesting that fetal LMPPs and CLPs share features with adult erythroid progenitors that are not directly linked to red blood cell production. Indeed, among the proteins significantly upregulated in fetal LMPPs and CLPs, translation- and/or proliferation-associated proteins Rrm1, Heatr3, Eif2s3x, Larp4, and Birc5 have high transcript expression in adult CFU-Es (Bagger et al., 2019). Similarly, ribosomal proteins, which are highly expressed in activated T cells (Bagger et al., 2019), potentially explain the relatively strong association of fetal LMPPs and CLPs to those cell subsets.

In accordance with proteins significantly upregulated in fetal GMPs showing enrichment for biological processes related to inflammation and coagulation (Figures 2G and S1H), the proteomic profile of these cells also showed a pronounced association

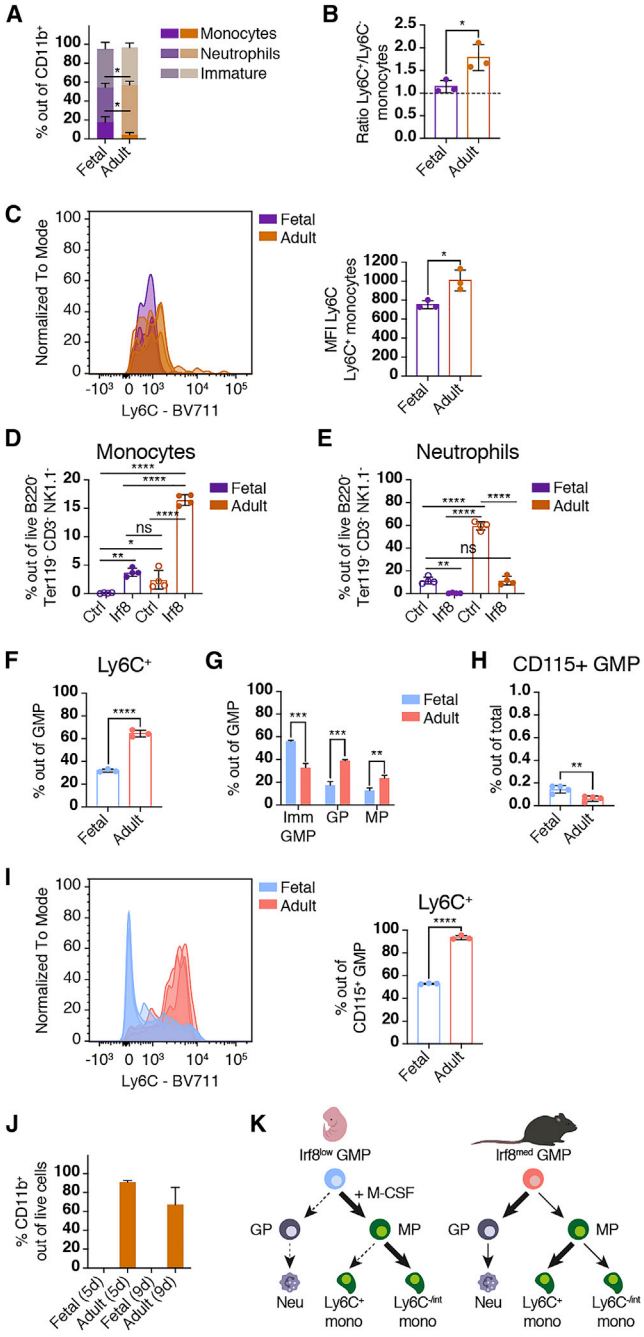

Figure 5. Differential expression of Irf8 correlates with ontogenic alterations in monocyte differentiation

(A) Frequency of neutrophils, monocytes, and immature myeloid cells (NK1.1$^-$ CD11c$^-$ CD11b$^+$ Ly6G$^-$ CD115$^-$) after 7-day suspension culture of fetal and adult GMPs. n = 3.

(B and C) Ratio of Ly6C$^+$ to Ly6C$^-$ monocytes (B) and Ly6C expression on Ly6C$^+$ monocytes (C) derived from *in vitro* cultured fetal and adult GMPs. n = 3.

(D and E) Frequency of monocytes (D) and neutrophils (E) produced from fetal and adult GMPs transduced with GFP (Ctrl) or Irf8-GFP (Irf8). n = 4.

(F) Frequency of Ly6C$^+$ cells within the fetal and adult GMP pool. n = 3.

(G) Frequency of Ly6C$^-$ CD115$^-$ immature GMPs, Ly6C$^+$ CD115$^-$ GPs and Ly6C$^+$ CD115$^+$ MPs within the fetal and adult GMP pool. n = 3. Imm, immature.

with megakaryocyte progenitors (MkPs) compared with that of their adult counterpart (Figure 4C). Strikingly, expression of megakaryocyte-erythroid (MegE)-associated proteins Itga2b (CD41) (Pronk et al., 2007), Paf (Foulks et al., 2009), and Ptgs1 (Haas et al., 2015) was increased in fetal relative to adult GMPs (Figure 4D), in line with our other observations of a possible retainment of MegE potential in fetal myeloid progenitors (Figures 2G, 4C, and S1H). Analysis of cell-surface CD41 levels confirmed significantly greater expression in fetal compared with adultGMPs (Figure 4E). Importantly, CD41 expression on fetal GMPs was still approximately 85% lower than that observed on MkPs (Figure 4F). To exclude the possibility that CD41$^+$ fetal cells representprimitive erythro-myeloid progenitors (EMPs) persisting from earlier waves of embryonic hematopoiesis (Gomez Perdiguero et al., 2015), we assessed the macrophage differentiation potential of the fetal cells. Although the frequency of granulocytes produced from CD41$^-$ relative to CD41$^+$ fetal GMPs was increased, both fractions generated equally low numbers of F4/80$^+$ macrophages (Figure S3E), confirming that CD41$^+$ fetal GMPs represent a population separate from EMPs. Because the frequency of immunophenotypic CD150$^+$ CD41$^+$ MkPs within the LS$^-$K population is greatly reduced in the FL relative to the ABM (Figure S3F), we next investigated whether GMPs may act as an alternative source of megakaryocytes during fetal life. Surprisingly, we found very limited megakaryocyte production from fetal or adult GMPs under either homeostatic or stressed conditions (Figure 4G). In summary, although the proteomic signatures of HPCs correlate with ontogenic alterations in myeloid potential, the shared proteomic features of fetal GMPs with MkPs, including increased expression of CD41, do not have any effect on the cells' ability to produce megakaryocytes.

Ontogeny-specific differences in Irf8 expression drive a diminished capacity for monocyte differentiation in fetal GMPs

An intriguing finding from our analysis of TFs and myelopoiesis-associated proteins was significantly increased expression of Irf8 in adult relative to fetal GMPs (Figures 2H and 4D). Loss of Irf8 has a severe effect on the generation of mature monocytes and is sufficient to produce a chronic myelogenous leukemia-like disease in mice (Kurotaki et al., 2013; Tamura et al., 2015; Yáñez et al., 2015). Considering this remarkably strong phenotype, we decided to explore the capacity for monocytic differentiation in fetal and adult GMPs. The frequency of myeloid cells produced was low from both fetal and adult GMPs, but was significantly greater from adult compared with fetal cells (Figure S3G). Although the frequency of monocytes and neutrophils produced within the B220$^-$ Ter119$^-$ CD3$^-$ NK1.1$^-$ population was equal between fetus and adult (Figures 1H and S3H), the CD11b$^+$ fraction displayed differential composition between

(H) Frequency of CD115$^+$ cells within the fetal and adult GMP population. n = 3.

(I) Ly6C expression on fetal and adult CD115$^+$ GMPs. n = 3.

(J) Frequency of CD11b$^+$ cells derived from fetal and adult CD115$^+$ GMPs. n = 3.

(K) Proposed model.

Error bars are ±SD. *p < 0.05, **p < 0.01, ***p < 0.001, ****p < 0.0001, ns, non-significant. See also Figure S3.

fetal and adult wells (Figure 5A). In contrast to what would be expected considering that Irf8 promotes monocytic cell fate, fetal GMPs produced significantly higher frequencies of monocytes than did adult GMPs, whereas the opposite was true for neutrophil generation (Figure 5A). However, upon analysis of expression of Ly6C, a marker for inflammatory monocytes (Gordon and Taylor, 2005), we found that the ratio of Ly6C$^+$ to Ly6C$^-$ monocytes was approximately 50% lower in fetal- relative to adult-derived cells (Figure 5B). Additionally, we observed an accumulation of CD11b$^-$ Ly6C$^+$ CD115$^+$ cells immunophenotypically analogous to monocyte progenitors (MPs) (Yáñez et al., 2015) in fetal GMP wells (Figure S3I). Furthermore, Ly6C$^+$ monocytes derived from fetal GMPs showed a significantly lower Ly6C surface expression relative to those produced from adult GMPs (Figure 5C), suggesting incomplete monocytic maturation and a partial block in monocyte differentiation in fetal GMPs. Importantly, this phenotype shares many similarities with that previously observed in adult *Irf8*$^{-/-}$ mice (Kurotaki et al., 2013; Yáñez et al., 2015). We next set out to investigate whether increasing Irf8 expression would promote monocyte differentiation in fetal GMPs. Strikingly, enforced expression of Irf8 in fetal GMPs resulted in an increased production of monocytes, with frequencies similar to adult control GMPs (Figure 5D). In line with the known role of Irf8 in promoting a monocytic over neutrophilic cell fate (Kurotaki et al., 2013; Tamura et al., 2015; Yáñez et al., 2015), we observed a reduction in neutrophil output from both fetal and adult Irf8-overexpressing GMPs relative to control cells (Figure 5E). However, although Irf8 overexpression increased production of Ly6C$^+$ monocytes from adult cells, no difference was observed in the output of Ly6C$^+$ monocytes from fetal Irf8-transduced relative to control GMPs (Figure S3J), indicating only partial reversal of the blockade in monocytic differentiation and maturation (Figures 5B, 5C, and S3I).

Because it has been suggested that Irf8 has its highest expression and main function in unipotent Ly6C$^+$ CD115$^-$ granulocyte progenitors (GPs) and Ly6C$^+$ CD115$^+$ MPs downstream of GMPs (Yáñez et al., 2015), we next evaluated the composition of the GMP population in the fetus and the adult based on these two markers. In contrast to adult GMPs, where 60%–70% of the GMP population expressed Ly6C, only 30% of the fetal GMP pool did (Figure 5F), although the absolute frequency of Ly6C$^+$ GMPs within the FL was slightly greater than the corresponding population in ABM (Figure S3K). Further subdivision of immunophenotypic GMPs into immature GMPs (Ly6C$^-$ CD115$^-$), GPs, and MPs confirmed a significantly lower frequency of GPs and MPs, and a significantly higher frequency of bipotent progenitors within the fetal GMP pool, relative to that of the adult (Figure 5G), indicating that the ABM environment more efficiently drives terminal myeloid differentiation than does the FL. In addition, the absolute frequency of immature GMPs in FL was approximately twice that of ABM (Figure S3L). However, we did find that the FL contains a larger population of CD115$^+$ GMPs than ABM (Figure 5H) and that only half of these cells additionally express Ly6C, whereas the adult CD115$^+$ GMP population almost exclusively consists of Ly6C$^+$ cells (Figure 5I). To further characterize the fetal and adult CD115$^+$ GMPs, we investigated the myeloid differentiation capacity of these cells. Strikingly, fetal CD115$^+$ GMPs failed to give rise to any live progeny (Figure 5H), indicating that CD115$^+$ GMPs in the FL represent terminally differentiated cells, despite half of the cells sharing the adult MP immunophenotype (Figure 5I). In stark contrast, 70%–90% of the progeny of adult CD115$^+$ GMPs already expressed CD11b after 5 days (Figure 5J), a far higher frequency than what we observed for unfractionated adult GMPs (Figure S3G). The progeny of adult CD115$^+$ GMPs exclusively consisted of monocytes, confirming that these cells represent unipotent MPs (Figure S3M).

Taken together, our data show that the lower Irf8 expression in fetal relative to adult GMPs results in an impaired monocytic differentiation capacity in fetal GMPs, which can be partially rescued by enhancing Irf8 expression (Figure 5K). The low expression of Irf8 additionally correlates with a diminished prevalence of Ly6C$^+$ unipotent myeloid progenitors in the fetal GMP pool compared with that of the adult (Figures 5F and 5G). Our results further reveal that CD115$^+$ GMPs in the fetus do not correspond to MPs in the adult and that *in situ* GMP-derived monopoiesis is not yet fully developed in the E14.5 FL.

DISCUSSION

In this work, we have comprehensively described the cellular proteome of, and functionally characterized, three subsets of lineage-biased HPCs in the fetus and adult. By keeping the extrinsic factors of the *in vitro* culture experiments identical for fetal and adult cells, we have been able to link the cells' differential functional potential to their intrinsic molecular differences.

We have uncovered that adult-specific features are conserved across the different hematopoietic cell lineages, whereas fetal-specific features differ between lymphoid-competent (LMPPs and CLPs) and myeloid-restricted (GMPs) progenitors. We have additionally found that proteins characterizing fetal LMPPs and CLPs belong to categories of features typically attributed to fetal hematopoiesis, such as a high proliferative and translational rate. In contrast, proteins distinguishing fetal from adult GMPs were enriched for considerably more processes that relate to differentiation capacity and lineage output. To some extent, the lack of a signature of proliferation and translation in fetal GMPs can likely be attributed to GMPs being closer to a terminally differentiated cell state, in which fetal and adult cells can be expected to exhibit similar proliferative behavior. Indeed, cell-cycle-related processes were even more apparent as fetal features in our proteome comparison of fetal and adult HSPCs (Jassinskaja et al., 2017). Furthermore, an additional explanation for the particularly strong ontogeny-specific features in lymphoid-competent HPCs is that B and T lymphopoiesis are known to have distinct fetal and adult features, with some innate-like lymphocytes being generated exclusively during fetal life (Bendelac et al., 2001; Elsaid et al., 2019; Hardy and Hayakawa, 1991).

Previous studies have reported more extensive myeloid potential and transcript-level multilineage priming in embryonic and fetal LMPPs compared with that of adult cells (Böiers et al., 2018; Boyer et al., 2011; Månsson et al., 2007; Schlenner et al., 2010; Welner et al., 2009). In contrast, our *in vitro* differentiation results and proteome data suggest a stronger association of adult LMPPs to the myeloid lineage. Direct comparisons to previous work are, however, obstructed by the use of a multitude

of different immunophenotypic definitions and lineage-potential assays across different studies, as well as discrepancies between transcript- and protein-level expression profiles. It is important to note that our functional assays should be regarded as a comparison of the cells' capacities driven by intrinsic factors. For example, the monocyte output we observed from adult CLPs do not fully represent the cells' *in vivo* lineage potential, as previously reported (Richie Ehrlich et al., 2011).

Undoubtedly, our study underscores the necessity to perform proteomic analyses to fully understand the biology of HPCs and potential leukemia-initiating cells. Indeed, the timing of the establishment of myelopoiesis has so far been left unresolved, possibly because of a lack of gene-expression profiling on the protein level (Rowe et al., 2016; Traver et al., 2001). Our data support the notion that HSC-derived myelopoiesis is not yet fully developed in the E14.5 FL and is subject to considerable ontogenic regulation (Rowe et al., 2016), which we have linked to differential expression of myelopoiesis-associated proteins. This includes that fetal GMPs express lower levels of Irf8 compared with their adult counterparts and produce monocytes with a phenotype reminiscent of that observed in adult *Irf8*$^{-/-}$ mice (Kurotaki et al., 2013; Yáñez et al., 2015), which can be partially rescued by increasing Irf8 expression in the fetal cells. Although we observed a significantly higher frequency of CD11b^{-} Ly6C^{+} CD115^{+} "MP-like" cells produced from fetal compared with adult GMPs *in vitro*, the FL did not contain an expanded MP population *in vivo*, in contrast to what has previously been reported for the BM of mice deficient in Irf8 (Yáñez et al., 2015). A potential explanation for this is that the FL environment appears to less strongly promote terminal myeloid differentiation relative to the ABM environment, as the fetal GMP pool contains far fewer immunophenotypic MPs and GPs than does the adult. Investigations of the role of cell-extrinsic factors are required to resolve this question.

Unexpectedly, although myosins are mostly associated with housekeeping roles, our data point toward an involvement of these proteins in regulating expansion and differentiation of both fetal and adult LMPPs and that fetal LMPPs are more sensitive than adult LMPPs to disruption of myosin activity. These initial results are in line with the previously reported leukemia-inhibitory effect of ROCK inhibition and MLC knockdown (Mali et al., 2011). Further detailed investigations are needed to conclude these indications and to resolve whether these potential effects are different between adult and *in utero*-derived leukemias.

Although fetal GMPs expressed lower levels of many proteins associated with myeloid commitment compared with adult GMPs, the expression of several proteins linked to a MegE fate were elevated in fetal relative to adult cells. Previous studies have identified similar trends when comparing fetal and adult CMPs, a heterogeneous population of cells that comprises myeloid as well as MegE progenitors (Rowe et al., 2016). However, although MegE-associated gene expression patterns in fetal and adult CMPs correlate with an enhanced capacity for generation of erythroid cells and granulocytes, respectively (Rowe et al., 2016), the shared protein signature of fetal GMPs with MkPs observed here does not confer on the fetal cells any substantial MegE potential. This indicates, rather, that the proteins that are typically associated with MegE fate represent a more general inflammatory signature and that fetal GMPs share more features with effector cells than they do with multipotent progenitors. This is supported by our functional assays, which show that the capacity for mature myeloid cell generation is lower from fetal compared to adult GMPs.

Collectively, our work has uncovered numerous molecular features that distinguish fetal and adult lineage-biased HPCs and raised important questions regarding the developmental timing of mature blood cell production from different hematopoietic progenitor populations. Our findings provide a substantial contribution to the current understanding of fetal and adult hematopoiesis. These results have nominated a host of proteins to test in future research focused on the development of age-tailored therapeutic approaches for improving the clinical outcomes of patients with infant and adult leukemia.

STAR★METHODS

Detailed methods are provided in the online version of this paper and include the following:

- KEY RESOURCES TABLE
- RESOURCE AVAILABILITY
  - Lead contact
  - Materials availability
  - Data and code availability
- EXPERIMENTAL MODEL AND SUBJECT DETAILS
  - Mice
  - Cell culture
- METHOD DETAILS
  - Flow cytometry and FACS
  - Sample preparation for proteome analysis
  - LC-MS analysis
  - OP9/OP9DI1 co-culture assays
  - Erythroid differentiation assay
  - Megakaryocyte differentiation assay
  - Suspension culture of GMPs
  - Lentiviral production
  - Viral transduction and Irf8 overexpression
  - ROCK and MLC kinase inhibition assays
- QUANTIFICATION AND STATISTICAL ANALYSIS
  - Protein identification and quantification
  - Statistical analysis

SUPPLEMENTAL INFORMATION

Supplemental Information can be found online at https://doi.org/10.1016/j.celrep.2021.108894.

ACKNOWLEDGMENTS

We acknowledge the personnel at the FACS Core Facility at Lund Stem Cell Center as well as Sven Kjellström and Hong Yan at the BioMS Lund node for their expert technical assistance. We thank Parashar Dhapola for assistance with generating radar plots and Fatemeh Safi and Charlotta Böiers for valuable input on experimental design. This work was supported by grants from the Swedish Research Council (to J.H.; 2015-03063) and The Swedish Childhood Cancer Foundation (to J.H.; TJ2106-0038).

AUTHOR CONTRIBUTIONS

J.H. and M.J. designed the study with input from E.S. and K.P. C.-F.P. designed Irf8-overexpression experiments together with J.H. and M.J. N.A. produced lentivirus under supervision of C.-F.P. M.J. performed experiments with assistance from K.P., E.J., and M.D. M.J. analyzed data. J.H. supervised the study. M.J. prepared the figures and wrote the paper together with J.H. and input from all authors.

DECLARATION OF INTERESTS

The authors declare no competing interests.

INCLUSION AND DIVERSITY

We worked to ensure sex balance in the selection of non-human subjects.

Received: September 1, 2020
Revised: December 16, 2020
Accepted: March 2, 2021
Published: March 23, 2021

REFERENCES

Adolfsson, J., Månsson, R., Buza-Vidas, N., Hultquist, A., Liuba, K., Jensen, C.T., Bryder, D., Yang, L., Borge, O.J., Thoren, L.A., et al. (2005). Identification of Flt3$^+$ lympho-myeloid stem cells lacking erythro-megakaryocytic potential a revised road map for adult blood lineage commitment. Cell *121*, 295–306.

Babovic, S., and Eaves, C.J. (2014). Hierarchical organization of fetal and adult hematopoietic stem cells. Exp. Cell Res. *329*, 185–191.

Bagger, F.O., Kinalis, S., and Rapin, N. (2019). BloodSpot: a database of healthy and malignant haematopoiesis updated with purified and single cell mRNA sequencing profiles. Nucleic Acids Res. *47* (*D1*), D881–D885.

Beerman, I., Seita, J., Inlay, M.A., Weissman, I.L., and Rossi, D.J. (2014). Quiescent hematopoietic stem cells accumulate DNA damage during aging that is repaired upon entry into cell cycle. Cell Stem Cell *15*, 37–50.

Bendelac, A., Bonneville, M., and Kearney, J.F. (2001). Autoreactivity by design: innate B and T lymphocytes. Nat. Rev. Immunol. *1*, 177–186.

Böiers, C., Richardson, S.E., Laycock, E., Zriwil, A., Turati, V.A., Brown, J., Wray, J.P., Wang, D., James, C., Herrero, J., et al. (2018). A human IPS model implicates embryonic B-myeloid fate restriction as developmental susceptibility to B acute lymphoblastic leukemia-associated ETV6-RUNX1. Dev. Cell *44*, 362–377.e7.

Boyer, S.W., Schroeder, A.V., Smith-Berdan, S., and Forsberg, E.C. (2011). All hematopoietic cells develop from hematopoietic stem cells through Flk2/Flt3-positive progenitor cells. Cell Stem Cell *9*, 64–73.

Carballo, E., Colomer, D., Vives-Corrons, J.L., Blackshear, P.J., and Gil, J. (1996). Characterization and purification of a protein kinase C substrate in human B cells: identification as lymphocyte-specific protein 1 (LSP1). J. Immunol. *156*, 1709–1713.

Dimayacyac-Esleta, B.R., Tsai, C.F., Kitata, R.B., Lin, P.Y., Choong, W.K., Lin, T.D., Wang, Y.T., Weng, S.H., Yang, P.C., Arco, S.D., et al. (2015). Rapid high-pH reverse phase stagetip for sensitive small-scale membrane proteomic profiling. Anal. Chem. *87*, 12016–12023.

Elsaid, R., Yang, J., and Cumano, A. (2019). The influence of space and time on the establishment of B cell identity. Biomed. J. *42*, 209–217.

Ema, H., and Nakauchi, H. (2000). Expansion of hematopoietic stem cells in the developing liver of a mouse embryo. Blood *95*, 2284–2288.

Feng, L., Gell, D.A., Zhou, S., Gu, L., Kong, Y., Li, J., Hu, M., Yan, N., Lee, C., Rich, A.M., et al. (2004). Molecular mechanism of AHSP-mediated stabilization of α-hemoglobin. Cell *119*, 629–640.

Foulks, J.M., Marathe, G.K., Michetti, N., Stafforini, D.M., Zimmerman, G.A., McIntyre, T.M., and Weyrich, A.S. (2009). PAF-acetylhydrolase expressed during megakaryocyte differentiation inactivates PAF-like lipids. Blood *113*, 6699–6706.

Gentleman, R.C., Carey, V.J., Bates, D.M., Bolstad, B., Dettling, M., Dudoit, S., Ellis, B., Gautier, L., Ge, Y., Gentry, J., et al. (2004). Bioconductor: open software development for computational biology and bioinformatics. Genome Biol. *5*, R80.

Georgouli, M., Herraiz, C., Crosas-Molist, E., Fanshawe, B., Maiques, O., Perdrix, A., Pandya, P., Rodriguez-Hernandez, I., Ilieva, K.M., Cantelli, G., et al. (2019). Regional activation of myosin II in cancer cells drives tumor progression via a secretory cross-talk with the immune microenvironment. Cell *176*, 757–774.e23.

Gomez Perdiguero, E., Klapproth, K., Schulz, C., Busch, K., Azzoni, E., Crozet, L., Garner, H., Trouillet, C., de Bruijn, M.F., Geissmann, F., and Rodewald, H.R. (2015). Tissue-resident macrophages originate from yolk-sac-derived erythro-myeloid progenitors. Nature *518*, 547–551.

Gordon, S., and Taylor, P.R. (2005). Monocyte and macrophage heterogeneity. Nat. Rev. Immunol. *5*, 953–964.

Greaves, M.F., Maia, A.T., Wiemels, J.L., and Ford, A.M. (2003). Leukemia in twins: lessons in natural history. Blood *102*, 2321–2333.

Haas, S., Hansson, J., Klimmeck, D., Loeffler, D., Velten, L., Uckelmann, H., Wurzer, S., Prendergast, A.M., Schnell, A., Hexel, K., et al. (2015). Inflammation-induced emergency megakaryopoiesis driven by hematopoietic stem cell-like megakaryocyte progenitors. Cell Stem Cell *17*, 422–434.

Han, H., Cho, J.W., Lee, S., Yun, A., Kim, H., Bae, D., Yang, S., Kim, C.Y., Lee, M., Kim, E., et al. (2018). TRRUST v2: an expanded reference database of human and mouse transcriptional regulatory interactions. Nucleic Acids Res. *46* (*D1*), D380–D386.

Hardy, R.R., and Hayakawa, K. (1991). A developmental switch in B lymphopoiesis. Proc. Natl. Acad. Sci. USA *88*, 11550–11554.

Huang, W., Sherman, B.T., and Lempicki, R.A. (2009). Systematic and integrative analysis of large gene lists using DAVID bioinformatics resources. Nat. Protoc *4*, 44–57.

Jacobs, M., Hayakawa, K., Swenson, L., Bellon, S., Fleming, M., Taslimi, P., and Doran, J. (2006). The structure of dimeric ROCK I reveals the mechanism for ligand selectivity. J. Biol. Chem. *281*, 260–268.

Jassinskaja, M., Johansson, E., Kristiansen, T.A., Åkerstrand, H., Sjöholm, K., Hauri, S., Malmström, J., Yuan, J., and Hansson, J. (2017). Comprehensive proteomic characterization of ontogenic changes in hematopoietic stem and progenitor cells. Cell Rep. *21*, 3285–3297.

Kadowaki, T., Yamaguchi, Y., Kido, M.A., Abe, T., Ogawa, K., Tokuhisa, M., Gao, W., Okamoto, K., Kiyonari, H., and Tsukuba, T. (2020). The large GTPase Rab44 regulates granule exocytosis in mast cells and IgE-mediated anaphylaxis. Cell. Mol. Immunol. *17*, 1287–1289.

Karsunky, H., Inlay, M.A., Serwold, T., Bhattacharya, D., and Weissman, I.L. (2008). Flk2$^+$ common lymphoid progenitors possess equivalent differentiation potential for the B and T lineages. Blood *111*, 5562–5570.

Kieusseian, A., Brunet de la Grange, P., Burlen-Defranoux, O., Godin, I., and Cumano, A. (2012). Immature hematopoietic stem cells undergo maturation in the fetal liver. Development *139*, 3521–3530.

Kim, P.G., Canver, M.C., Rhee, C., Ross, S.J., Harriss, J.V., Tu, H.C., Orkin, S.H., Tucker, H.O., and Daley, G.Q. (2016). Interferon-α signaling promotes embryonic HSC maturation. Blood *128*, 204–216.

Klimmeck, D., Hansson, J., Raffel, S., Vakhrushev, S.Y., Trumpp, A., and Krijgsveld, J. (2012). Proteomic cornerstones of hematopoietic stem cell differentiation: distinct signatures of multipotent progenitors and myeloid committed cells. Mol. Cell. Proteomics *11*, 286–302.

Kulak, N.A., Pichler, G., Paron, I., Nagaraj, N., and Mann, M. (2014). Minimal, encapsulated proteomic-sample processing applied to copy-number estimation in eukaryotic cells. Nat. Methods *11*, 319–324.

Kurotaki, D., Osato, N., Nishiyama, A., Yamamoto, M., Ban, T., Sato, H., Nakabayashi, J., Umehara, M., Miyake, N., Matsumoto, N., et al. (2013). Essential role of the IRF8-KLF4 transcription factor cascade in murine monocyte differentiation. Blood *121*, 1839–1849.

Kusumawidjaja, G., Kayed, H., Giese, N., Bauer, A., Erkan, M., Giese, T., Hoheise, J.D., Friess, H., and Kleeff, J. (2007). Basic transcription factor 3 (BTF3) regulates transcription of tumor-associated genes in pancreatic cancer cells. Cancer Biol. Ther. *6*, 367–376.

Loughran, S.J., Kruse, E.A., Hacking, D.F., de Graaf, C.A., Hyland, C.D., Willson, T.A., Henley, K.J., Ellis, S., Voss, A.K., Metcalf, D., et al. (2008). The transcription factor Erg is essential for definitive hematopoiesis and the function of adult hematopoietic stem cells. Nat. Immunol. *9*, 810–819.

Ma, W., Xia, C., Ling, P., Qiu, M., Luo, Y., Tan, T.H., and Liu, M. (2001). Leukocyte-specific adaptor protein Grap2 interacts with hematopoietic progenitor kinase 1 (HPK1) to activate JNK signaling pathway in T lymphocytes. Oncogene *20*, 1703–1714.

Mali, R.S., Ramdas, B., Ma, P., Shi, J., Munugalavadla, V., Sims, E., Wei, L., Vemula, S., Nabinger, S.C., Goodwin, C.B., et al. (2011). Rho kinase regulates the survival and transformation of cells bearing oncogenic forms of KIT, FLT3, and BCR-ABL. Cancer Cell *20*, 357–369.

Manesia, J.K., Franch, M., Tabas-Madrid, D., Nogales-Cadenas, R., Vanwelden, T., Van Den Bosch, E., Xu, Z., Pascual-Montano, A., Khurana, S., and Verfaillie, C.M. (2017). Distinct molecular signature of murine fetal liver and adult hematopoietic stem cells identify novel regulators of hematopoietic stem cell function. Stem Cells Dev. *26*, 573–584.

Månsson, R., Hultquist, A., Luc, S., Yang, L., Anderson, K., Kharazi, S., Al-Hashmi, S., Liuba, K., Thorén, L., Adolfsson, J., et al. (2007). Molecular evidence for hierarchical transcriptional lineage priming in fetal and adult stem cells and multipotent progenitors. Immunity *26*, 407–419.

McKinney-Freeman, S., Cahan, P., Li, H., Lacadie, S.A., Huang, H.T., Curran, M., Loewer, S., Naveiras, O., Kathrein, K.L., Konantz, M., et al. (2012). The transcriptional landscape of hematopoietic stem cell ontogeny. Cell Stem Cell *11*, 701–714.

Meyer, C., Burmeister, T., Gröger, D., Tsaur, G., Fechina, L., Renneville, A., Sutton, R., Venn, N.C., Emerenciano, M., Pombo-de-Oliveira, M.S., et al. (2018). The MLL recombinome of acute leukemias in 2017. Leukemia *32*, 273–284.

Mezzapesa, A., Bastelica, D., Crescence, L., Poggi, M., Grino, M., Peiretti, F., Panicot-Dubois, L., Dupont, A., Valero, R., Maraninchi, M., et al. (2019). Increased levels of the megakaryocyte and platelet expressed cysteine proteases stefin A and cystatin A prevent thrombosis. Sci. Rep. *9*, 9631.

Mi, H., Muruganujan, A., Ebert, D., Huang, X., and Thomas, P.D. (2019). PANTHER version 14: more genomes, a new PANTHER GO-slim and improvements in enrichment analysis tools. Nucleic Acids Res. *47* (*D1*), D419–D426.

Mikkola, H.K., and Orkin, S.H. (2006). The journey of developing hematopoietic stem cells. Development *133*, 3733–3744.

Morrison, S.J., Hemmati, H.D., Wandycz, A.M., and Weissman, I.L. (1995). The purification and characterization of fetal liver hematopoietic stem cells. Proc. Natl. Acad. Sci. USA *92*, 10302–10306.

Ng, A.P., Loughran, S.J., Metcalf, D., Hyland, C.D., de Graaf, C.A., Hu, Y., Smyth, G.K., Hilton, D.J., Kile, B.T., and Alexander, W.S. (2011). Erg is required for self-renewal of hematopoietic stem cells during stress hematopoiesis in mice. Blood *118*, 2454–2461.

Ng, A.P., Coughlan, H.D., Hediyeh-Zadeh, S., Behrens, K., Johanson, T.M., Low, M.S.Y., Bell, C.C., Gilan, O., Chan, Y.C., Kueh, A.J., et al. (2020). An Erg-driven transcriptional program controls B cell lymphopoiesis. Nat. Commun. *11*, 3013.

Nimmo, R.A., May, G.E., and Enver, T. (2015). Primed and ready: understanding lineage commitment through single cell analysis. Trends Cell Biol. *25*, 459–467.

Owen, H.R., Elser, M., Cheung, E., Gersbach, M., Kraus, W.L., and Hottiger, M.O. (2007). MYBBP1a is a novel repressor of NF-kappaB. J. Mol. Biol. *366*, 725–736.

Pietras, E.M., Reynaud, D., Kang, Y.A., Carlin, D., Calero-Nieto, F.J., Leavitt, A.D., Stuart, J.M., Göttgens, B., and Passegué, E. (2015). Functionally distinct subsets of lineage-biased multipotent progenitors control blood production in normal and regenerative conditions. Cell Stem Cell *17*, 35–46.

Pronk, C.J., Rossi, D.J., Månsson, R., Attema, J.L., Norddahl, G.L., Chan, C.K., Sigvardsson, M., Weissman, I.L., and Bryder, D. (2007). Elucidation of the phenotypic, functional, and molecular topography of a myeloerythroid progenitor cell hierarchy. Cell Stem Cell *1*, 428–442.

Raffel, S., Klimmeck, D., Falcone, M., Demir, A., Pouya, A., Zeisberger, P., Lutz, C., Tinelli, M., Bischel, O., Bullinger, L., et al. (2020). Quantitative proteomics reveals specific metabolic features of acute myeloid leukemia stem cells. Blood *136*, 1507–1519.

Rauniyar, N., and Yates, J.R., 3rd. (2014). Isobaric labeling-based relative quantification in shotgun proteomics. J. Proteome Res. *13*, 5293–5309.

Rebel, V.I., Miller, C.L., Eaves, C.J., and Lansdorp, P.M. (1996). The repopulation potential of fetal liver hematopoietic stem cells in mice exceeds that of their liver adult bone marrow counterparts. Blood *87*, 3500–3507.

Richie Ehrlich, L.I., Serwold, T., and Weissman, I.L. (2011). In vitro assays misrepresent in vivo lineage potentials of murine lymphoid progenitors. Blood *117*, 2618–2624.

Rosa, F.F., Pires, C.F., Kurochkin, I., Ferreira, A.G., Gomes, A.M., Palma, L.G., Shaiv, K., Solanas, L., Azenha, C., Papatsenko, D., et al. (2018). Direct reprogramming of fibroblasts into antigen-presenting dendritic cells. Sci. Immunol. *3*, eaau4292.

Rosa, F.F., Pires, C.F., Zimmermanova, O., and Pereira, C.F. (2020). Direct reprogramming of mouse embryonic fibroblasts to conventional type 1 dendritic cells by enforced expression of transcription factors. Bio Protoc. *10*, e3619.

Rowe, R.G., Wang, L.D., Coma, S., Han, A., Mathieu, R., Pearson, D.S., Ross, S., Sousa, P., Nguyen, P.T., Rodriguez, A., et al. (2016). Developmental regulation of myeloerythroid progenitor function by the Lin28b-let-7-Hmga2 axis. J. Exp. Med. *213*, 1497–1512.

Saitoh, M., Ishikawa, T., Matsushima, S., Naka, M., and Hidaka, H. (1987). Selective inhibition of catalytic activity of smooth muscle myosin light chain kinase. J. Biol. Chem. *262*, 7796–7801.

Schlenner, S.M., Madan, V., Busch, K., Tietz, A., Läufle, C., Costa, C., Blum, C., Fehling, H.J., and Rodewald, H.R. (2010). Fate mapping reveals separate origins of T cells and myeloid lineages in the thymus. Immunity *32*, 426–436.

Scott, L.M., Civin, C.I., Rorth, P., and Friedman, A.D. (1992). A novel temporal expression pattern of three C/EBP family members in differentiating myelomonocytic cells. Blood *80*, 1725–1735.

Sinha, S., Bheemsetty, V.A., and Inamdar, M.S. (2018). A double helical motif in OCIAD2 is essential for its localization, interactions and STAT3 activation. Sci. Rep. *8*, 7362.

Sun, J., He, X., Zhu, Y., Ding, Z., Dong, H., Feng, Y., Du, J., Wang, H., Wu, X., Zhang, L., et al. (2018). SIRT1 activation disrupts maintenance of myelodysplastic syndrome stem and progenitor cells by restoring TET2 function. Cell Stem Cell *23*, 355–369.e9.

Supek, F., Bošnjak, M., Škunca, N., and Šmuc, T. (2011). REVIGO summarizes and visualizes long lists of gene ontology terms. PLoS ONE *6*, e21800.

Tamura, T., Kurotaki, D., and Koizumi, S. (2015). Regulation of myelopoiesis by the transcription factor IRF8. Int. J. Hematol. *101*, 342–351.

Traver, D., Miyamoto, T., Christensen, J., Iwasaki-Arai, J., Akashi, K., and Weissman, I.L. (2001). Fetal liver myelopoiesis occurs through distinct, prospectively isolatable progenitor subsets. Blood *98*, 627–635.

Tyanova, S., Temu, T., Sinitcyn, P., Carlson, A., Hein, M.Y., Geiger, T., Mann, M., and Cox, J. (2016). The Perseus computational platform for comprehensive analysis of (prote)omics data. Nat. Methods *13*, 731–740.

Ugale, A., Norddahl, G.L., Wahlestedt, M., Säwén, P., Jaako, P., Pronk, C.J., Soneji, S., Cammenga, J., and Bryder, D. (2014). Hematopoietic stem cells are intrinsically protected against MLL-ENL-mediated transformation. Cell Rep. *9*, 1246–1255.

Velten, L., Haas, S.F., Raffel, S., Blaszkiewicz, S., Islam, S., Hennig, B.P., Hirche, C., Lutz, C., Buss, E.C., Nowak, D., et al. (2017). Human haematopoietic stem cell lineage commitment is a continuous process. Nat. Cell Biol. *19*, 271–281.

Welner, R.S., Esplin, B.L., Garrett, K.P., Pelayo, R., Luche, H., Fehling, H.J., and Kincade, P.W. (2009). Asynchronous RAG-1 expression during B lymphopoiesis. J. Immunol. *183*, 7768–7777.

Yáñez, A., Ng, M.Y., Hassanzadeh-Kiabi, N., and Goodridge, H.S. (2015). IRF8 acts in lineage-committed rather than oligopotent progenitors to control neutrophil vs monocyte production. Blood *125*, 1452–1459.

Yu, Y., Wang, J., Khaled, W., Burke, S., Li, P., Chen, X., Yang, W., Jenkins, N.A., Copeland, N.G., Zhang, S., and Liu, P. (2012). Bcl11a is essential for lymphoid development and negatively regulates p53. J. Exp. Med. *209*, 2467–2483.

Zaro, B.W., Noh, J.J., Mascetti, V.L., Demeter, J., George, B., Zukowska, M., Gulati, G.S., Sinha, R., Flynn, R.A., Banuelos, A., et al. (2020). Proteomic analysis of young and old mouse hematopoietic stem cells and their progenitors reveals post-transcriptional regulation in stem cells. eLife *9*, e62210.

Zhang, C.C., and Lodish, H.F. (2004). Insulin-like growth factor 2 expressed in a novel fetal liver cell population is a growth factor for hematopoietic stem cells. Blood *103*, 2513–2521.

Zhou, Y., Li, Y.S., Bandi, S.R., Tang, L., Shinton, S.A., Hayakawa, K., and Hardy, R.R. (2015). Lin28b promotes fetal B lymphopoiesis through the transcription factor Arid3a. J. Exp. Med. *212*, 569–580.

STAR★METHODS

KEY RESOURCES TABLE

REAGENT or RESOURCE	SOURCE	IDENTIFIER
Antibodies		
Rat anti-mouse Ter119 – PE-Cy5 (clone TER-119)	BioLegend	Cat#116210, RRID:AB_313711
Rat anti-mouse Ter119 – Biotin (clone TER-119)	BioLegend	Cat#116204, RRID:AB_313705
Rat anti-mouse Sca-1 – PE-Cy7 (clone D7)	BioLegend	Cat#108114, RRID:AB_493596
Mouse anti-mouse NK1.1 – PE-Cy5 (clone PK136)	BioLegend	Cat#108716, RRID:AB_493590
Rat anti-mouse Ly6G – PE-Cy7 (clone 1A8)	BioLegend	Cat#127618, RRID:AB_1877261
Rat anti-mouse Ly6C – BV711 (clone HK1.4)	BioLegend	Cat#128037, RRID:AB_2562630
Rat anti-mouse Ly6C – BV421 (clone HK1.4)	BioLegend	Cat#128031, RRID:AB_2562177
Rat anti-mouse Gr-1 – PE-Cy5 (clone RB6-8C5)	BioLegend	Cat#108410, RRID:AB_313375
Rat anti-mouse Gr-1 – APC (clone RB6-8C5)	BioLegend	Cat#108412, RRID:AB_313377
Rat anti-mouse Gr-1 – Biotin (clone RB6-8C5)	BioLegend	Cat#108403, RRID:AB_313368
Rat anti-mouse F4/80 – Pacific Blue (clone BM8)	BioLegend	Cat#123123, RRID:AB_893487
Rat anti-mouse CD90.2 – PE (clone 53-2.1)	BioLegend	Cat#140308, RRID:AB_10641145
Rat anti-mouse CD8α – APC-Cy7 (clone 53-6.7)	BioLegend	Cat#100713, RRID:AB_312752
Rat anti-mouse CD63 – APC (clone NVG-2)	BioLegend	Cat#143906, RRID:AB_2565496
Rat anti-mouse CD5 – BV605 (clone 53-7.3)	BD Biosciences	Cat#563194, RRID:AB_2738061
Rat anti-mouse CD41 – BV605 (clone MWReg30)	BioLegend	Cat#133921, RRID:AB_2563933
Rat anti-mouse CD4 – PE-Cy7 (clone RM4-5)	BioLegend	Cat#100527, RRID:AB_312728
Armenian hamster anti-mouse CD3ε – PE-Cy5 (clone 145-2C11)	BioLegend	Cat#100310, RRID:AB_312675
Armenian hamster anti-mouse CD3ε – Biotin (clone 145-2C11)	BioLegend	Cat#100303, RRID:AB_312668
Rat anti-mouse CD3 – Pacific Blue (clone 17A2)	BioLegend	Cat#100214, RRID:AB_493645
Rat anti-mouse CD25 – APC (clone PC61)	BioLegend	Cat#102012, RRID:AB_312861
Rat anti-mouse CD19 – FITC (clone 1D3/CD19)	BioLegend	Cat#152404, RRID:AB_2629813
Rat anti-mouse CD19 – BV650 (clone 6D5)	BioLegend	Cat#115541, RRID:AB_11204087
Rat anti-mouse CD16/32 – PE (clone 93)	BioLegend	Cat#101308, RRID:AB_312807
Rat anti-mouse CD16/32 (Fc block)	BD Biosciences	Cat#553142, RRID:AB_394657
Rat anti-mouse CD150 – BV605 (clone TC15-12F12.2)	BioLegend	Cat#115927, RRID:AB_11204248
Rat anti-mouse CD150 – BV785 (clone TC15-12F12.2)	BioLegend	Cat#115937, RRID:AB_2565962
Rat anti-mouse CD135 (Flt3) – BV421 (clone A2F10)	BioLegend	Cat#135315, RRID:AB_2571919
Rat anti-mouse CD127 (IL-7Rα) – PE (clone A7R34)	BioLegend	Cat#135010, RRID:AB_1937251
Armenian hamster anti-mouse CD11c – BV421 (clone N418)	BioLegend	Cat#117343, RRID:AB_2563099
Rat anti-mouse CD11b – PE-Cy5 (clone M1/70)	BioLegend	Cat#101210, RRID:AB_312793
Rat anti-mouse CD11b – PE (clone M1/70)	BioLegend	Cat#101208, RRID:AB_312791
Rat anti-mouse CD11b – Biotin (clone M1/70)	BioLegend	Cat#101203, RRID:AB_312786
Rat anti-mouse cKit – BV421 (clone 2B8)	BioLegend	Cat#105827, RRID:AB_10898120
Rat anti-mouse cKit (CD117) – APC (clone 2B8)	BioLegend	Cat#105812, RRID:AB_313221
Rat anti-mouse B220 – PE-Cy5 (clone RA3-6B2)	BioLegend	Cat#103210, RRID:AB_312995

(*Continued on next page*)

Continued

REAGENT or RESOURCE	SOURCE	IDENTIFIER
Rat anti-mouse B220 – Biotin (clone RA3-6B2)	BioLegend	Cat#103203, RRID:AB_312988
Rat anti-mouse B220 – BV421 (clone RA3-6B2)	BD Biosciences	Cat#562922, RRID:AB_2737894
Rat anti-mouse CD115 – APC-Cy7 (clone AFS98)	BioLegend	Cat#135531, RRID:AB_2632739
Bacterial and virus strains		
Competent *E. coli* DH5α	NEB	Cat#C2987I
Chemicals, peptides, and recombinant proteins		
Rho kinase (ROCK) inhibitor H-1152	R&D Systems	Cat#871543-07-6
Myosin light chain (MLC) kinase inhibitor ML-9	Merck	Cat#C1172
Recombinant mouse IFNα	Miltenyi	Cat#130-093-131
Mouse recombinant SCF	StemCell Technologies	Cat#78064
Mouse recombinant Flt3-ligand	StemCell Technologies	Cat#78011
Mouse recombinant M-CSF	StemCell Technologies	Cat#78059
Mouse recombinant TPO	StemCell Technologies	Cat#78072
Mouse recombinant GM-CSF	StemCell Technologies	Cat#78017
Human recombinant IL-6	StemCell Technologies	Cat#78050
Mouse recombinant IL-3	StemCell Technologies	Cat#78042
Human recombinant IL-7	StemCell Technologies	Cat#78053
Human recombinant G-CSF	StemCell Technologies	Cat#78012
EPO	Laboratory of Dr. Göran Karlsson	N/A
7AAD	Merck	Cat#SML1633
TMT6plex reagents	Thermo Scientific	Cat#10322094
Polyethylenimine transfection reagent	Sigma-Aldrich	Cat#408727
Hexadimethrine bromide (Polybrene)	Sigma-Aldrich	Cat# H9268
Critical commercial assays		
iST – NHS kit	PreOmics	Cat#P.O.00026
Lenti-X Concentrator	Takara	Cat#631232
MegaCult-C Collagen and Medium Without Cytokines	StemCell Technologies	Cat#04960
Deposited data		
Raw proteome data	This paper	MassIVE: MSV000085672
Microarray data	ImmGen https://www.immgen.org	GEO: GSE15907; samples proB.CLP.BM#1, proB.CLP.BM#6, proB.CLP.BM#8, proB.CLP.FL#1, proB.CLP.FL#2, proB.CLP.FL#3
Experimental models: cell lines		
Human: HEK293T	ATCC	Cat#CRL-3216
Mouse: OP9	Laboratories of Profs. Ewa Sitnicka and David Bryder	N/A
Mouse: OP9DL1	Laboratory of Prof. Ewa Sitnicka	N/A
Experimental models: organisms/strains		
Mouse: C57BL/6NTac (MPF, genotype B6-none)	Taconic Bioscience	Cat#B6-F and B6-M
Mouse: C57BL/6N	In-house breeding	N/A
Recombinant DNA		
pRRL.PPT.SFFV_MCS.IRES.GFP	This paper	N/A

(*Continued on next page*)

Continued

REAGENT or RESOURCE	SOURCE	IDENTIFIER
pRRL.PPT.SFFV_IRF8.IRES.GFP	This paper	N/A
Software and algorithms		
FlowJo	BD Biosciences	https://www.flowjo.com/
Prism	GraphPad	https://www.graphpad.com/scientific-software/prism/
Proteome Discoverer	Thermo Scientific	https://www.thermofisher.com/order/catalog/product/OPTON-30812#/OPTON-30812
Perseus	Tyanova et al., 2016	https://maxquant.net/perseus/
Limma package	Gentleman et al., 2004	https://bioconductor.org/packages/release/bioc/html/limma.html
PANTHER	Mi et al., 2019	http://www.pantherdb.org/
DAVID	Huang et al., 2009	https://david.ncifcrf.gov/
REVIGO	Supek et al., 2011	http://revigo.irb.hr/
BloodSpot	Bagger et al., 2019	http://servers.binf.ku.dk/bloodspot/
TRRUST	Han et al., 2018	https://www.grnpedia.org/trrust/

RESOURCE AVAILABILITY

Lead contact

Requests for further information should be directed to and will be fulfilled by the lead contact, Jenny Hansson (jenny.hansson@med.lu.se).

Materials availability

Irf8 construct will be made available upon request.

Data and code availability

Proteome data have been deposited to ProteomeXchange via the repository MassIVE: MSV000085672.

EXPERIMENTAL MODEL AND SUBJECT DETAILS

Mice

Wild-type C57BL/6N mice purchased from Taconic Biosciences or bred in-house were used for all experiments. All experiments involving animals were performed in accordance with ethical permits approved by the Swedish Board of Agriculture. Animals were housed in individually ventilated cages (IVC) and provided with sterile food and water *ad libitum*. Adult mice used in all experiments were 6-10 weeks old. E14.5 embryos were obtained by timed pregnancies overnight. The morning after mating was considered E0.5. For proteome analysis, equal numbers of male and female mice were used. For all other experiments, a mix of male and female mice were used.

Cell culture

OP9 and OP9DL1 murine stromal cell lines were stored at −150°C in freezing media containing 10% DMSO (Merck). Cells were thawed by briefly placing vials in a water bath at 37°C. Cells were seeded at 300,000-500,000 cells per flask in 80 or 175 cm^3 culture flasks (Thermo Scientific) in 20 mL OptiMem + GlutaMAX media (GIBCO) supplemented with 10% fetal calf serum (FCS; HyClone), 1% penicillin/streptomycin (GIBCO) and 0.02% 50 mM 2-mercaptoethanol (GIBCO; hereafter termed complete medium). Cells were maintained in an incubator at 37°C and 5% CO_2 and passaged upon reaching 80% confluency (approximately every 48-72 hours). Passaging of cells was performed by incubation with trypsin (HyClone) for 4 min at 37°C. Flasks were washed twice with complete medium to retrieve detached cells prior to centrifugation for 5 min at 400xg at room temperature (RT) and reseeding.

METHOD DETAILS

Flow cytometry and FACS

Adult bone marrow (ABM) was extracted from hind limbs, hip bones, forelimbs, shoulders, sternum and spine collected in Hank's Balanced Salt Solution (HBSS; HyClone) supplemented with 0.5% bovine serum albumin (BSA) and 2 mM EDTA (hereafter termed collection media). Single-cell suspension of ABM was obtained by crushing bones using a mortar and pestle and passing cell

suspensions through a 40 μm filter. Red blood cells were lysed by incubating ABM cells with ammonium chloride solution (StemCell Technologies) for 2 minutes on ice. Lineage-positive cells were removed from ABM cell suspension by depletion for Gr-1 (RB6-8C5; BioLegend), Ter119 (TER119; BioLegend), CD3 (145-2C11; BioLegend), B220 (RA3-652; BioLegend) and CD11b (M1/70; BioLegend) using biotin-conjugated antibodies at a concentration of 0.1 μl/10^6 cells with MACS anti-biotin beads at a concentration of 1 μl/10^6 cells using the autoMACS Pro Separator (Miltenyi Biotech) or LS columns (Miltenyi Biotech). Fetal livers (FLs) were extracted from embryos collected at E14.5 gestation into collection media. Single-cell suspension of FLs was obtained by mechanical dissociation and passing through a 40 μm filter. Red cells were removed from FL cell suspensions by depletion for Ter119 using a biotin-conjugated antibody with MACS anti-biotin beads using the autoMACS Pro Separator or LS columns. Depletion and red blood cell lysis was omitted in experiments where frequencies are reported out of total cells. FL and ABM cells were surface-stained with fluorophore-conjugated antibodies against either Sca-1 (1 μg/ml; D7; BioLegend), c-Kit (1 μg/ml; 2B8; BioLegend), Gr-1 (0.5 μg/ml), Ter119 (0.5 μg/ml), CD3 (0.5 μg/ml), B220 (0.5 μg/ml), Flt3 (2 μg/ml; A2F10; BioLegend), IL-7Rα (2 μg/ml; A7R34; BioLegend) and CD150 (1 μg/ml; TC15-12F12.2; BioLegend; LMPP/CLP cocktail), or Sca-1, c-Kit, Gr-1, Ter119, CD3, B220, CD41 (1 μg/ml; MWReg30; BioLegend), CD150 and CD16/32 (2 μg/ml; 93; BioLegend; GMP cocktail). Anti-Ly6c (1 μg/ml; HK1.4; BioLegend), -CD115 (2 μg/ml; AFS98; BioLegend) and -CD63 (2 μg/ml; NVG-2; BioLegend) were included in the GMP antibody cocktail for experiments where the GMP population was resolved into MPs and GPs. Adult cells were additionally stained for CD11b (0.5 μg/ml). In all flow cytometry and FACS experiments, cells were incubated with 7AAD (Merck) briefly before analysis to exclude dead cells. All flow cytometry and FACS experiments were performed on BD FACSAriaIIu (70 μm nozzle), BD FACSAriaIII (70 or 85 μm nozzle), BD LSRFortessa or BD LSRFortessa X-20 instruments at the FACS Core Facility at Lund Stem Cell Center. Data analysis was performed in FlowJo (BD).

Sample preparation for proteome analysis

FACS-sorted cells were collected in ice-cold HBSS, centrifuged and stored as dry pellets at −80°C until further use. Pellets corresponding to 100,000 cells were processed using in-StageTip (iST) NHS sample preparation kit (PreOmics) in accordance with manufacturer's protocol. Digested peptides were labeled using TMT6plex reagents (Thermo Scientific) in accordance with manufacturer's protocol. Immediately before use, TMT6plex reagents were equilibrated to RT. Vials containing 0.8 mg of TMT label were dissolved in 41 μL of anhydrous acetonitrile (ACN). Labeling was performed by addition of 10 μL dissolved TMT6plex to each sample and incubation for 1 hour at RT. Labeling reagents were swapped in the second and third biological replicate. Following desalting, labeled peptides were combined and dried by vacuum centrifugation. High-pH-reverse phase (HpH-RP) pre-fractionation was carried out as previously described (Dimayacyac-Esleta et al., 2015) with some modifications. HpH-RP columns were assembled by packing C18-AQ beads onto 4 layers of C8 membrane in a 200 μL pipette tip via centrifugation. Columns were conditioned and equilibrated by sequential addition of 100% methanol followed by 80% and 20.8% ACN in ammonium formate, and finally 100% ammonium formate. Dried peptides were dissolved in 100% ammonium formate and bound to the column by centrifugation. HpH-RP pre-fractionation was carried out by sequential elution into 13 fractions containing increasing concentrations of ACN in ammonium formate: 7.5% (F1), 9% (F2), 11% (F3), 12.5% (F4), 14.5% (F5), 17.5% (F6), 20.8% (F7), 25% (F8), 28% (F9), 30% (F10), 35% (F11), 40% (F12), and 80% (F13). To achieve an even distribution of peptides in LC-MS analysis, fractions were combined as follows: F1+F9, F2+F10, F3+F11, F4+F12, and F5+F13 (yielding a total of 8 fractions together with F6, F7 and F8 that were kept separate). Fractionated samples were dried by vacuum centrifugation and stored at −20°C until further use. Prior to LC-MS analysis, samples were dissolved in 4% ACN/0.1% formic acid (FA).

LC-MS analysis

MS analyses were carried out on an Orbitrap Fusion Tribrid MS instrument (Thermo Scientific) equipped with a Proxeon Easy-nLC 1000 (Thermo Fisher) using a 120 min linear gradient separation followed by a synchronous precursor selection (SPS)-MS3 method. Each fraction was injected twice. Injected peptides were trapped on an Acclaim PepMap C18 column (3 μm particle size, 75 μm inner diameter x 20 mm length, nanoViper fitting), followed by gradient elution of peptides on an Acclaim PepMap RSLC C18 100 Å column (2 μm particle size, 75 μm inner diameter x 250 mm length, nanoViper fitting) using 0.1% (v/v) FA in LC-MS-grade water (solvent A) and 0.1% (v/v) FA in ACN (solvent B) as the mobile phases. Peptides were loaded with a constant flow of solvent A at 9 μl/min onto the trapping column and eluted via the analytical column at a constant flow of 300 nl/min. During the elution step, the percentage of solvent B was increased in a linear fashion from 5% to 10% in 2 minutes, followed by an increase to 25% in 85 minutes and finally to 60% in an additional 20 minutes. The peptides were introduced into the mass spectrometer via a Stainless-Steel Nano-bore emitter (150 μm OD x 30 μm ID; 40 mm length; Thermo Scientific) using a spray voltage of 2.0 kV. The capillary temperature was set at 275°C. Data acquisition was carried out using a data-dependent SPS-MS3 method. The full MS scan was performed in the Orbitrap in the range of 380 to 1580 m/z and at a resolution of 120,000 at full-width-half-max (FWHM) using an automatic gain control (AGC) of 4.0e5 and a maximum ion accumulation time of 50 ms. The most intense ions (up to ten) selected in the first MS scan were isolated for ion trap collision-induced dissociation (CID)-MS2 at a precursor isolation window width of 0.7 m/z, an AGC of 1.5e4, a maximum ion accumulation time of 50 ms and a resolution of 30,000 FWHM. The normalized collision energy was set to 35%. The precursor selection range for MS3 was set to an m/z range of 400–1200 in MS2. Orbitrap higher-energy collisional dissociation (HCD)-MS3 scans were acquired in parallel mode with synchronous precursor selection (up to ten precursors), a normalized collision energy of 55% and a resolution of 15,000 FWHM in a range of 100–500 m/z. The fragment ion isolation width was set to 2 m/z, the AGC was 1.0e5 and the maximum injection time 120 ms.

OP9/OP9Dl1 co-culture assays

For coculture experiments, 50 fetal and adult HPCs were FACS-sorted into 48-well plates onto pre-established layers of 10,000 OP9/OP9DL1 cells per well. Cells were cultured in complete medium supplemented with 25 ng/mL stem cell factor (SCF), 25 ng/mL Flt3-ligand (Flt3l), 20 ng/mL interleukin (IL) −7, 10 ng/mL IL-6, 10 ng/mL granulocyte (G) -colony stimulating factor (CSF), 10 ng/mL granulocyte-macrophage (GM)-CSF and 10 ng/mL IL-3 (OP9), or 25 ng/mL SCF and 25 ng/mL Flt3l (OP9DL1). SCF was omitted after the first week of culture for OP9DL1 co-cultures. All cytokines were purchased from Stem Cell Technologies. Prior to flow cytometric analysis, cultured cells were incubated with anti-CD16/32 (BD Biosciences) as FC-block and stained with fluorophore-conjugated antibodies against NK1.1 (0.5 μg/ml; PK136; BioLegend), CD11c (0.5 μg/ml; N418; BioLegend), Ly6G (0.5 μg/ml; 1A8; BioLegend), Ly6C (0.5 μg/ml), CD11b (1 μg/ml), CD19 (1 μg/ml; 6D5 or 1D3/CD19; BioLegend), B220 (2 μg/ml) and CD115 (2 μg/ml), or CD25 (1 μg/ml; PC61; BioLegend), Thy1 (0.3 μg/ml; 53-2.1; BioLegend), CD3 (1 μg/ml), CD4 (1 μg/ml; RM4-5; BioLegend) and CD8 (1 μg/ml; 53-6.7; BioLegend). Anti-F4/80 (2.5 μg/ml; BM8; BioLegend) and anti-Gr-1 (1 μg/ml; in place for Ly6G) were used when investigating the lineage-potential of fetal $CD41^-$ and $CD41^+$ GMPs.

Erythroid differentiation assay

Erythroid potential was evaluated by culturing 10 fetal and adult cells per well in Terasaki plates in X-VIVO 15 medium (Lonza) supplemented with 0.5% BSA, 10% FCS, 100 U/mL penicillin/streptomycin, 2 mM L-glutamine (GIBCO), 0.1 mM 2-mercaptoethanol, 50 ng/mL SCF, 50 ng/mL Flt3L, 20 ng/mL IL-3, 30 ng/mL thrombopoietin (TPO) and 5 U/mL erythropoietin (EPO, which was generously provided by Dr. Göran Karlsson). Erythroid colony formation was assessed by diaminofluorene (DAF) staining.

Megakaryocyte differentiation assay

Fetal and adult GMPs were suspension cultured at 5,000 cells per well in complete medium supplemented with 50 ng/mL TPO, 20 ng/mL IL-6 and 10 ng/mL IL-3. IFNα (3,125 U; Miltenyi Biotech) or sterile water was added to stress and control wells, respectively. Cells were collected after 16 hours and megakaryocyte potential was assessed using the MegaCult culture system (StemCell Technologies) in accordance with manufacturer's protocol.

Suspension culture of GMPs

Suspension cultures of fetal and adult myeloid progenitors were performed by culturing 5,000 fetal and adult cells per well in round-bottom plates in complete medium supplemented with 25 ng/mL SCF, 10 ng/mL IL-6, 10 ng/mL IL-3, and 10 ng/mL macrophage (M)-CSF. Cells were cultured for 7-9 days. Cultured cells were incubated with FC-block and stained with fluorophore-conjugated antibodies against Ter119, CD3, B220, NK1.1, CD11c, CD11b, CD115, Ly6G and Ly6C prior to flow cytometric analysis.

Lentiviral production

HEK293T cells were co-transfected with a mixture of transfer plasmid, packaging and VSV-G encoding envelope constructs with polyethyleneimine as previously described (Rosa et al., 2018, 2020). Viral supernatants were harvested after 36, 48 and 72 hours, filtered (0.45 μm, low protein-binding), concentrated 40-fold with Lenti-X Concentrator (Takara) and stored at −80°C until further use.

Viral transduction and Irf8 overexpression

10,000 fetal and adult GMPs per well were cultured in round-bottom plates in complete media supplemented with 25 ng/mL SCF, 10 ng/mL IL-6, 10 ng/mL IL-3, 10 ng/mL M-CSF and 8 mg/ml polybrene. Cells were incubated overnight with 18 μL SFFV-MCS-IRES-GFP or SFFV-IRF8-IRES-GFP lentiviral particles. Media was exchanged after transduction to remove polybrene and any remaining viral particles. The following day, 5,500 GFP^+ cells per sample were FACS-sorted and seeded into round-bottom plates in complete media supplemented with 25 ng/mL SCF, 10 ng/mL IL-6, 10 ng/mL IL-3, 10 ng/mL M-CSF. Cells were cultured for an additional 5 days. Cultured cells were incubated with FC-block and stained with fluorophore-conjugated antibodies against Ter119, CD3, B220, NK1.1, CD11c, CD11b, CD115, Ly6G, Ly6C and cKit prior to flow cytometric analysis.

ROCK and MLC kinase inhibition assays

50 fetal and adult LMPPs were co-cultured with OP9 cells as described above. For ROCK inhibition experiments, ROCK inhibitor H1152 (2 μM; R&D systems) or sterile water was added to wells at the start of culture and again 24 hours later. Media was exchanged after 48 hours to remove any remaining H1152. For experiments involving IFNα, cells were cultured in the presence of IFNα (31.25 U) or sterile water for 18 hours prior to media exchange and addition of H1152. Cells were cultured for an additional 4-12 days before analysis. For MLC kinase inhibition experiments, cells were cultured in the presence of 50 or 100 μM ML-9 (Merck) for 24 hours prior to reseeding on fresh OP9 stroma. Cultured cells were incubated with FC-block and stained with fluorophore-conjugated antibodies against NK1.1, Gr-1, CD11b, CD19, B220 and CD5 (1 μg/ml; 53-7.3; BD Biosciences) prior to flow cytometric analysis. Cell number and viability was assessed with trypan blue using an automated cell counter (BioRad).

QUANTIFICATION AND STATISTICAL ANALYSIS

Protein identification and quantification

MS raw data were processed with Proteome Discoverer (version 2.2.0; Thermo Scientific). Enzyme was set to trypsin and a maximum of two missed cleavages were allowed. Cysteine acetylhypusinylation and N-terminal and lysine TMT6plex were set as static modifications. Methionine oxidation and N-terminal acetylation were set as dynamic modifications. The peak list was searched using the Sequest HT node against the Swissprot mouse data base (version 2017.07.05; 25,170 protein entries) together with commonly observed contaminants and reversed sequences for all entries. An FDR of 1% was required for identification at both the peptide and the protein level. Precursor and fragment mass tolerance were set to 10 ppm and 0.6 Da, respectively. Unique and razor peptides were used for quantification. The co-isolation threshold was set to 75. Proteins were quantified based on the average corrected TMT reporter ion intensities from two technical replicates per sample. Data was normalized by adjusting the median of each channel to the median of the medians of the entire replicate. Principal component analysis (PCA) was performed on the average protein abundances for each cell type using Perseus (version 1.6.6.0) (Tyanova et al., 2016). Correlation was assessed using the Pearson correlation coefficient. Statistical analysis was performed on ratios of normalized intensities using the Limma package in R/Bioconductor (Gentleman et al., 2004). P values were corrected for multiple testing using Benjamini-Hochberg's method. Proteins with an adjusted p value < 0.05 were considered to be differentially expressed. The PANTHER classification system was used to retrieve classification of proteins (Mi et al., 2019). For differentially expressed proteins, gene ontology (GO) enrichment analysis was performed using the functional annotation tool DAVID (Huang et al., 2009). Redundant GO terms were filtered out using REVIGO (Supek et al., 2011). Analysis of transcription factor (TF) expression was performed on proteins classified as TFs by PANTHER and validated as TFs by TRRUST (Han et al., 2018). Mapping of differentially expressed proteins to transcriptome data from BloodSpot was carried out using the "normal mouse hematopoiesis" dataset. A radar plot was generated using min-max scaled median values of marker genes in each cell type.

Statistical analysis

For all other experiments, differences between groups were assessed by two-tailed Students' t test (two groups) or one-way ANOVA with Tukey's post hoc test (three or more groups) using Prism software version 8 (GraphPad). Error bars represent SD. ****$p < 0.0001$, ***$p < 0.001$, **$p < 0.01$, and *$p < 0.05$ and ns = non-significant.

Cell Reports, Volume *34*

Supplemental information

Ontogenic shifts in cellular fate are linked to proteotype changes in lineage-biased hematopoietic progenitor cells

Maria Jassinskaja, Kristýna Pimková, Nejc Arh, Emil Johansson, Mina Davoudi, Carlos-Filipe Pereira, Ewa Sitnicka, and Jenny Hansson

SUPPLEMENTAL FIGURES AND FIGURE LEGENDS

Figure S1

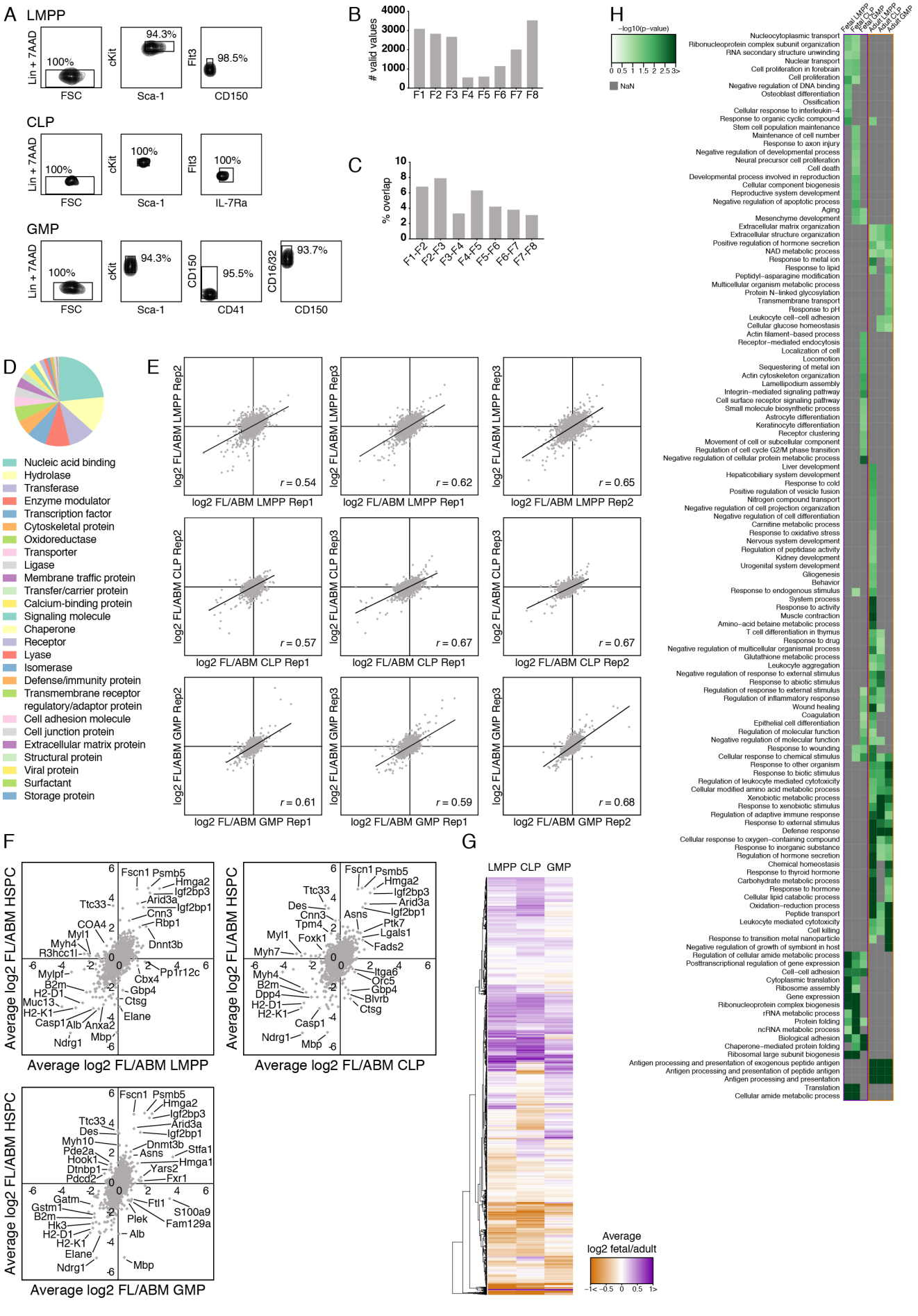

Figure S1. Comprehensive protein-level characterization of fetal and adult LMPPs, CLPs and GMPs. Related to Figures 1 and 2. (A) Representative FACS plots showing purity of sorted LMPPs, CLPs and GMPs. (B, C) Number of peptides quantified in each of the eight HpH-RP fractions analyzed by MS (B) and overlap between peptides identified in adjacent fractions (C) from six replicates of 100,000 FACS-sorted LS$^-$K cells. (D) PANTHER classification of the 4189 identified proteins. Proteins from 26 different classes were identified. (E) Protein expression correlation between the three replicates shown as the Pearson correlation coefficient (*r*). (F) Correlation between fetal/adult LMPP, CLP and GMP protein ratios and fetal/adult HSPC protein ratios. (G) Heatmap showing average expression of 4021 proteins quantified in both the fetus and the adult in all three cell types. n=3. (H) Heatmap depicting enrichment (-log10 p-value) of all biological processes identified as enriched among differentially expressed proteins in any cell type. Only processes with a p-value < 0.05 are shown. Processes that were not detected are depicted in grey. n=3.

Figure S2

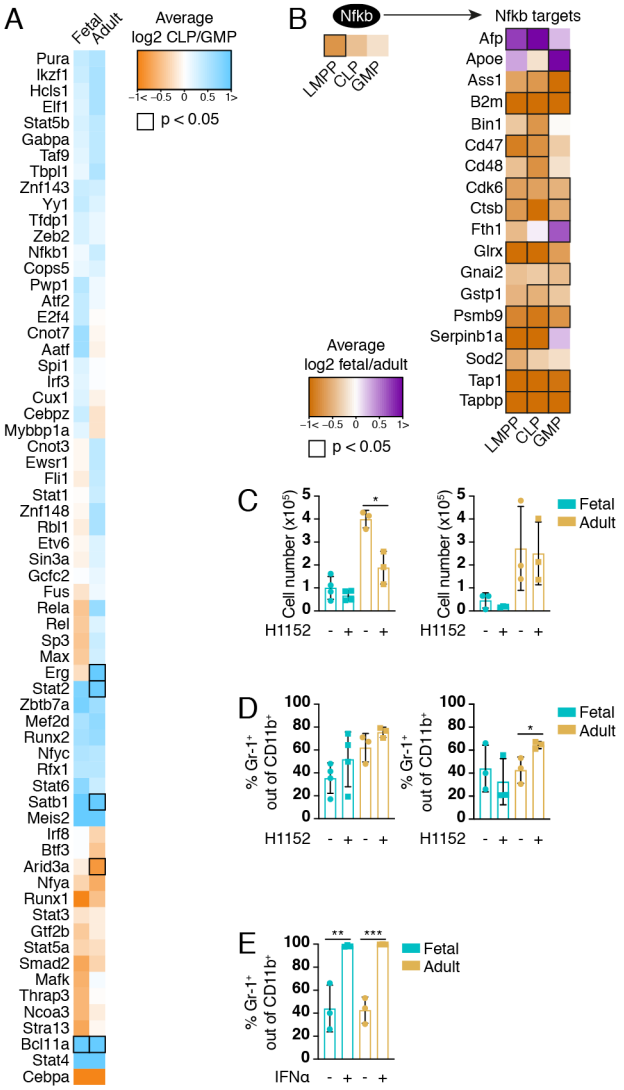

Figure S2. Protein expression differences indicate differential functionality of fetal and adult HPCs. Related to Figures 2 and 3. (A) Heatmap depicting the relative expression of proteins classified as transcription factors by PANTHER and validated by TRRUST. Proteins differentially expressed between CLPs and GMPs are indicated by a black frame. Data represent the average of three biological replicates. (B) Protein expression of Nfkb and its targets in fetal and adult LMPPs, CLPs, and GMPs. Differentially expressed proteins are indicated by a black frame. n=3. (C, D) Cell count (C) and frequency of Gr-1$^+$ granulocytes (D) following treatment with H1152. The two panels represent two different experiments. n=3-4 for fetal and n=3 for adult. (E) Frequency of Gr-1+ granulocytes derived from LMPPs treated with IFNa. n=3. Error bars are ± SD. *p<0.05, **p<0.01 and ***p<0.001.

Figure S3

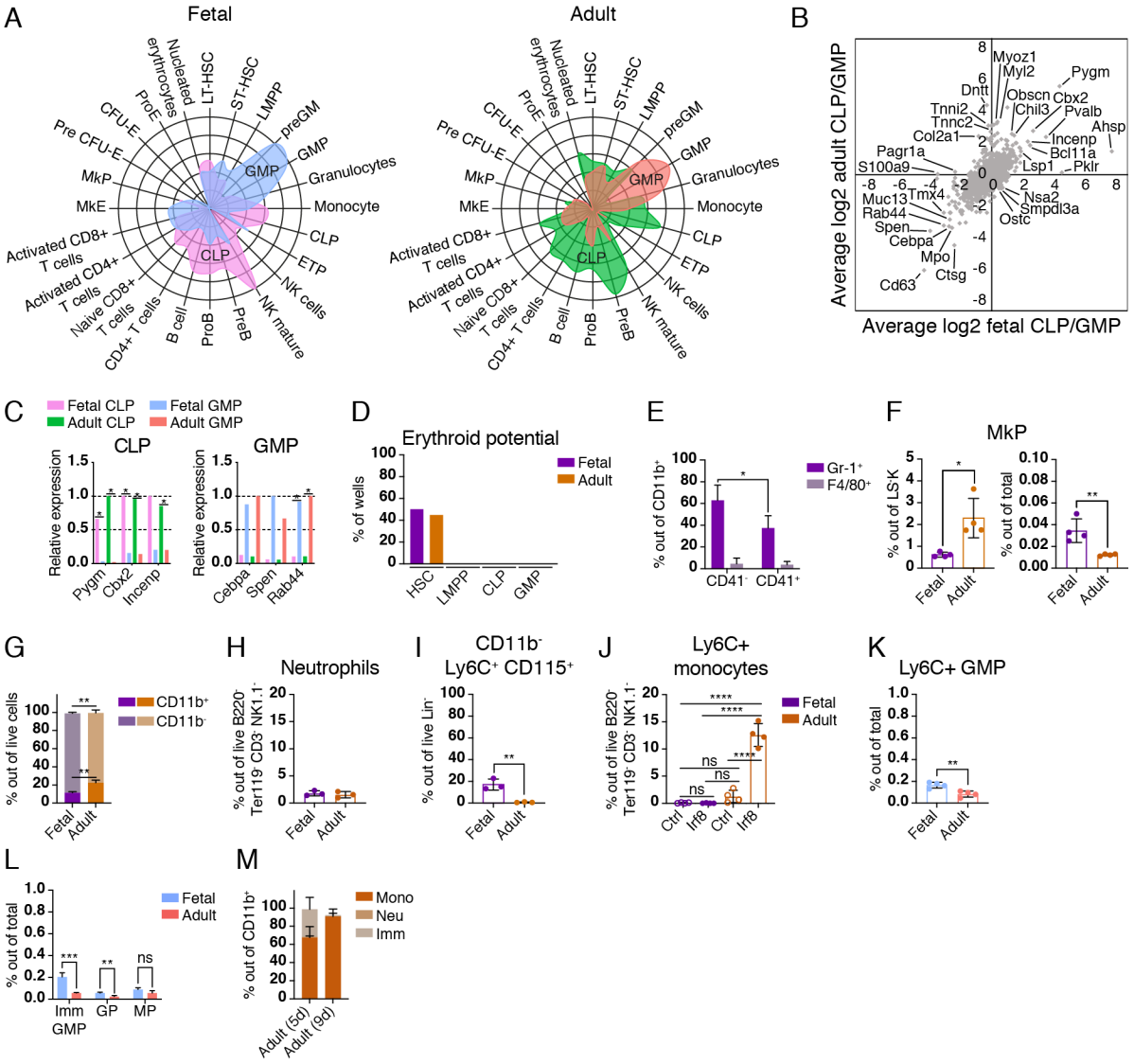

Figure S3. Expression of lineage-associated proteins predicts potential of fetal and adult HPCs. Related to Figures 4 and 5. (A) Radar plots depicting the association of differentially expressed proteins in CLPs and GMPs with known transcriptional profiles of murine hematopoietic cell subsets. (B) Correlation between fetal CLP/GMP and adult CLP/GMP protein ratios. (C) Relative expression of proteins identified as CLP and GMP signature proteins in (B). Data represent the average of three biological replicates. (D) Erythroid potential in fetal and adult LMPPs, CLPs and GMPs. HSCs were included as a positive control. (E) In vitro granulocyte (NK1.1$^-$ CD11b$^+$ Gr-1$^+$ F4/80$^-$) and macrophage (NK1.1$^-$ CD11b$^+$ Gr-1$^-$ F4/80$^+$) potential of fetal CD41$^-$ and CD41$^+$ GMPs. n=3. (F) Frequency of MkPs (LS$^-$K CD41$^+$ CD150$^+$) in E14.5 FL and ABM. n=4. (G) Frequency of CD11b$^+$ and CD11b$^-$ cells derived from fetal and adult GMPs. n=3. (H) Frequency of neutrophils derived from fetal and adult GMPs. n=3.

(I) Frequency of CD11b^{-} Ly6C^{+} CD115^{+} cells immunophenotypically analogous to MPs derived from fetal and adult GMPs. n=3. (J) Frequency of Ly6C^{+} monocytes derived from fetal and adult GMPs transduced with GFP (Ctrl) or GFP-Irf8 (Irf8). n=4. (K, L) Absolute frequency of Ly6C^{+} GMPs (K) and immature (Imm) GMPs, GPs and MPs (L) within E14.5 FL and ABM n=3. (M) Frequency of neutrophils, monocytes and immature myeloid cells derived from adult CD115^{+} GMPs. n=3. Error bars are ± SD. *p<0.05, **p<0.01, ***p<0.001, ****p<0.0001 and ns=non-significant.